Economic Geology
Vol. 93, 1998, pp. 651–670

Controls of Alteration and Mineralization in the Sungun Porphyry Copper Deposit, Iran: Evidence from Fluid Inclusions and Stable Isotopes

ARDESHIR HEZARKHANI[†] AND ANTHONY E. WILLIAMS-JONES

Department of Earth and Planetary Sciences, McGill University, 3450 University Street, Montreal, Quebec, Canada H3A 2A7

Abstract

The Sungun porphyry copper deposit is located in northwestern Iran (Azarbaijan province) and is associated with diorite-granodiorite to quartz monzonite of Miocene age which intruded Eocene volcano-sedimentary and Cretaceous carbonate rocks. Copper mineralization was accompanied by both potassic and phyllic alteration. Field observations and petrographic studies demonstrate that emplacement of the Sungun stock took place in several intrusive pulses, each with associated hydrothermal activity. Molybdenum was concentrated at a very early stage in the evolution of the hydrothermal system and copper somewhat later. Four main vein groups have been identified: (I) quartz + molybdenite + anhydrite ± K feldspar with minor pyrite, chalcopyrite, and bornite; (II) quartz + chalcopyrite + pyrite ± molybdenite; (III) quartz + pyrite + calcite ± chalcopyrite ± anhydrite (gypsum) ± molybdenite; and (IV) quartz ± calcite ± gypsum ± pyrite. Early hydrothermal alteration produced a potassic assemblage (orthoclase-biotite) in the central part of the stock, propylitic alteration occurred contemporaneously with potassic alteration, but in the peripheral parts of the stock, and phyllic alteration occurred later, overprinting the earlier alteration. The early hydrothermal fluids are represented by high-temperature (340°– 500°C), high-salinity (up to 60 wt % NaCl equiv) liquid-rich fluid inclusions, and high-temperature (320°–550°C), low-salinity, vapor-rich inclusions. These fluids are interpreted to represent an orthomagmatic fluid which boiled episodically; the brines are interpreted to have caused potassic alteration and deposition of group I and II quartz veins containing molybdenite and chalcopyrite. Propylitic alteration is attributed to a liquid-rich, lower temperature (240°–330°C), Ca-rich, evolved meteoric fluid. Influx of meteoric water into the central part of the system and mixing with magmatic fluid produced deep albitization (transition alteration) and shallow phyllic alteration. This influx also caused dissolution of early formed copper sulfides and remobilization of Cu into the sericitic zone where it was redeposited in response to a boiling-induced decrease in temperature. Supergene alteration was minor and restricted to a thin blanket of Cu sulfides below an argillic cap.

Introduction

ALTHOUGH porphyry copper deposits have been intensively studied in the Mesozoic-Cenozoic orogenic belts of the American Cordillera and East Pacific rim (e.g., Sillitoe, 1973; Gustafson and Hunt, 1975; Titley and Beane, 1981) and their genesis is relatively well understood, there have been few investigations of this style of mineralization in Iran and southern Asia. In Iran, all known porphyry copper mineralization occurs in the Cenozoic Sahand-Bazman orogenic belt (Fig. 1). This belt was formed by subduction of the Arabian plate beneath central Iran during the Alpine orogeny (Niazi and Asoudeh, 1978; Berberian and King, 1981; Pourhosseini, 1981) and hosts two major porphyry Cu deposits. The Sar-Cheshmeh deposit is the only one of these being mined and contains 450 Mt of sulfide ore with an average grade of 1.13 percent Cu and ~0.03 percent Mo (Waterman and Hamilton, 1975). The Sungun deposit, which contains >500 Mt of sulfide reserves grading 0.76 percent Cu and ~0.01 percent Mo (unpublished data of the Iranian Copper Company), is currently being developed. Sar-Cheshmeh, Sungun, and a number of subeconomic porphyry copper deposits are all associated with mid- to late Miocene diorite-granodiorite to quartz monzonite stocks (Shahabpour, 1982; Emami, 1992).

The Sungun deposit area was first described by Bazin and Hübner (1969), who reported skarn-type mineralization at the contact between Cretaceous limestone and the granodioritic stock. On the basis of the overall geologic setting and alteration patterns, Etminan (1977) proposed that the Sungun Cu deposit is porphyry related. Mehrpartou (1993) subsequently made a preliminary study of the igneous petrology and fluid inclusions, and concluded that the overall characteristics of the deposit are very similar to those predicted by the generalized porphyry deposit model of Lowell and Guilbert (1970). However, these studies have not provided sufficient data to evaluate the evolution of the mineralizing system and establish a genetic model.

The purpose of this paper is to elucidate the hydrothermal history of the Sungun porphyry deposit and identify the factors controlling Cu ± Mo mineralization. To aid us in this task we have (1) documented the alteration and vein mineral paragenesis by a combination of field mapping, core logging, and microscopic examination of polished thin sections, (2) conducted a fluid inclusion study; (3) analyzed the major and trace element, and isotopic compositions of selected minerals, and (4) evaluated mineral stabilities and solubilities. This information has enabled us to determine the conditions under which the deposit formed, to reconstruct the fluid evolution, and to develop a model which satisfactorily explains the concentration of Cu mineralization to economic levels. By comparing the results from this study with data available from Sar-Cheshmeh and porphyry copper deposits in other parts of the world, we have been able to achieve a better understanding of the nature of Sahand-Bazman porphyry copper province.

[†] Corresponding author: ardeshir@geosci.lan.mcgill.ca

0361-0128/98/1990/651-20$6.00

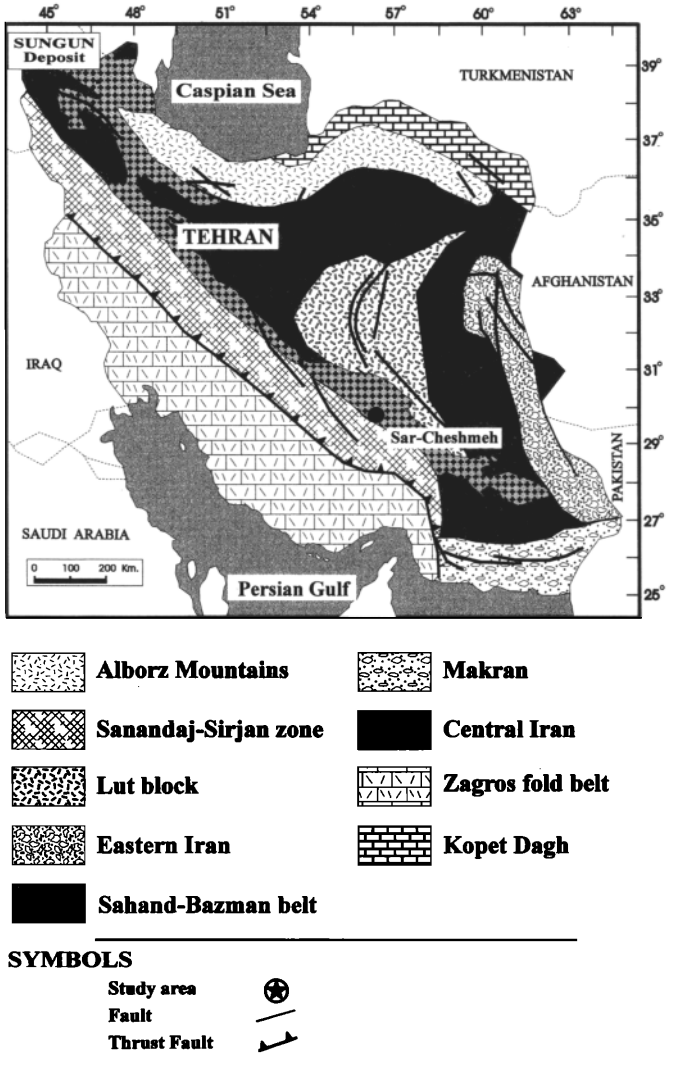

FIG. 1. Geologic map of Iran (modified from Stöcklin, 1977, and Shahabpour, 1994) showing major lithotectonic units as follows. Zagros fold belt: Paleozoic platform sediments overlain by miogeosynclinal mid-Triassic to Miocene sediments and synorogenic Pliocene-Pleistocene conglomerates; Sanandaj-Sirjan zone: Mesozoic granodioritic intrusions and metamorphosed Mesozoic sediments; Central Iran zone: Paleozoic platform sediments disrupted by late Triassic tectonic activity, and including horsts of Precambrian crystalline basement and Cambrian to Triassic cover rocks; Sahand-Bazman belt: calc-alkaline volcanic, quartz monzonite, and quartz diorite intrusions of dominantly Miocene age, hosting Cu-Mo porphyry-style mineralization; Lut block: the Lut block is considered to be an old stable platform (Stöcklin and Setudenia, 1972; Stöckline, 1977), covered by thick Mesozoic sediments and Eocene volcanics; Alborz Mountains and Kopeh Dagh zones: Eocene volcanic and volcanoclastic rocks in the Alborz segment, and in the Kopeh-Dagh segment; and the Eastern Iran and Makran zones: post-Cretaceous flysch-mollasse sediments.

Geologic Setting of the Sungun Deposit

The Sungun porphyry copper deposit is hosted by a diorite-granodiorite to quartz monzonite stock (Mehrpartou, 1993), located 75 km northwest of Ahar in the Azarbaijan province of northwestern Iran (Fig. 1). The stock is part of the Sahand-Bazman igneous and metallogenic belt (northern Iran), a deeply eroded Tertiary volcanic field, roughly 100 by 1,700 km in extent (from Turkey to Baluchistan in southern Iran), consisting mainly of rhyolite and andesite, with numerous felsic intrusions. The volcanics were laid down unconformably over folded and eroded Upper Cretaceous andesitic volcanic and sedimentary rocks (~500 m thick). Subduction and subsequent continental collision during the Paleocene to Oligocene caused extensive alkaline and calc-alkaline volcanic and plutonic igneous activity (Etminan, 1978; Shahabpour, 1982; Berberian, 1983), including intrusion of a porphyritic calc-alkaline stock at Sungun during the Miocene (Emami, 1992). Bordering the belt to the southwest is a major zone of complexly folded, faulted, and metamorphosed Tertiary and Paleozoic sedimentary rocks which form the Zagros Mountains (Waterman and Hamilton, 1975).

Sungun Stock and Peripheral Intrusive Rocks

The Sungun stock is a complex intrusive body, which crops out over an area of about 1.5 by 2.3 km (Fig. 2). The stock consists of three different intrusive phases: (1) monzonite-quartz monzonite, (2) diorite-granodiorite, and (3) andesite and related dikes, listed in order of emplacement (Mehrpartou, 1993; Hezarkhani, 1997). The monzonite-quartz monzonite is volumetrically the most important and includes most of the western part of the intrusive complex at the current erosional surface. The diorite-granodiorite is volumetrically the next most important and hosts most of the mineralization. These two intrusive phases are cut by monzonitic and andesitic dikes, which in the northern and eastern parts of the Sungun stock are also locally mineralized. Petrographic studies have shown that mineralized dikes are mainly andesitic and are related to the diorite-granodiorite intrusive phase. The diorite-granodiorite and monzonite-quartz monzonite contain some mafic xenoliths, whereas xenoliths are rare in the mineralized dikes.

The Sungun diorite-granodiorite intrudes Cretaceous limestones (~500 m thickness) and lower Tertiary volcanic and related sedimentary rocks (~1,000 to ~1,500 m thickness). The latter consist of andesitic to trachytic tuff and agglomerates, with intercalated marly tuff. Quaternary trachytic to andesitic lavas are exposed locally to the west and south of the deposit. They are unaltered and contain no known mineralization.

The Sungun stock is highly altered, and even in the outermost part of the intrusion it is not possible to find completely fresh rock. Metasomatic effects are also evident in the country rocks, particularly in the eastern part, where limestone has been altered to garnet-pyroxene and amphibole-epidote skarns containing disseminated pyrite, chalcopyrite, sphalerite, and galena, together with calcite, quartz, and magnetite.

Petrographic Observations of the Stock

Petrographic observations of polished thin sections indicate that monzonitic and quartz-monzonitic rocks contain 60 to 70 vol percent phenocrysts including up to 30 vol percent of K feldspar phenocrysts. The other important phenocryst phases are quartz (up to 20%) and plagioclase (up to 25%). Plagioclase (An_{17-35}) appears to have been the first of these phenocryst minerals to crystallize, as indicated by the common occurrence of euhedral to subhedral inclusions of plagioclase in K feldspar and quartz. Accessory minerals include magnetite, apatite, zircon, monazite, scheelite, titanite, urani-

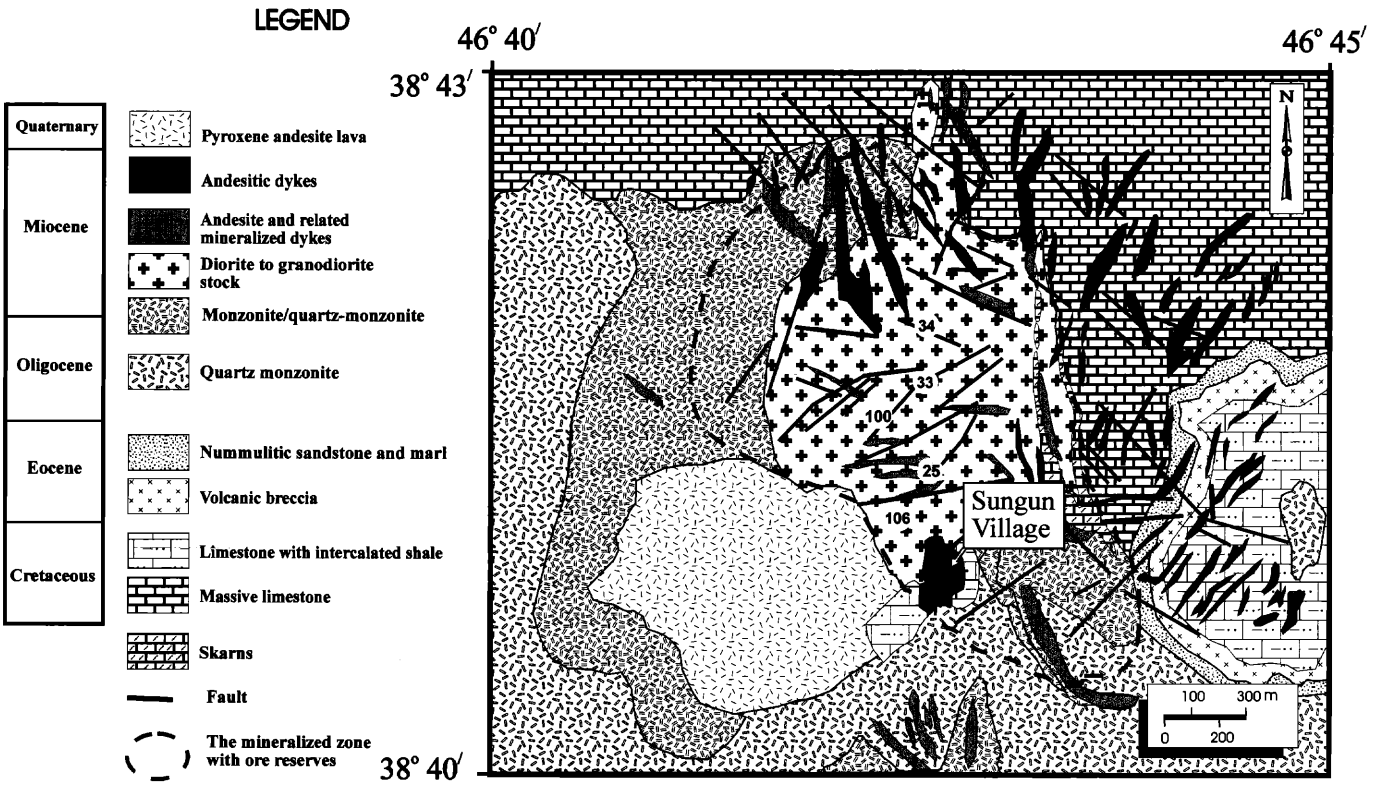

FIG. 2. Detailed geologic map of the Sungun area showing the distribution of different igneous suites (modified from Mehrpartou, 1993). Numbers on map refer to locations of drill holes that were sampled.

nite, and rutile, which occur as inclusions in the silicate phases and interstitial to them. The diorite-granodiorite contains ~50 percent by volume of phenocrysts consisting mainly of zoned plagioclase (An_{15-32}), highly altered hornblende, quartz, and biotite; it is distinguished from the monzonite-quartz monzonite by the lack of K feldspar phenocrysts. Hornblende was the earliest major mineral to crystallize and forms euhedral to subhedral phenocrysts. Quartz phenocrysts crystallized next and are ubiquitously rounded or embayed, which is a (predicted) consequence of isothermal decompression of a water vapor-undersaturated magma (Whitney, 1989). Plagioclase phenocrysts (mainly subhedral) formed shortly after the quartz phenocrysts, and biotite phenocrysts (subhedral to anhedral) formed late. The diorite-granodiorite groundmass is fine grained and consists mainly of quartz, plagioclase, and K feldspar, with lesser biotite and amphibole. Apatite, zircon, scheelite, titanite, uraninite, and rutile are present in minor to trace amounts.

Dikes consist mainly of plagioclase (An_{22-27}), K feldspar, biotite, quartz, and highly altered amphibole. Plagioclase occurs both as microcrystals in the groundmass and phenocrysts (up to 10 mm in diam) and composes more than 40 percent of the total volume of the rock unit. K feldspar crystals compose up to 30 vol percent of the total volume of the rock and occur both as phenocrysts and in the groundmass. Amphibole occurs only as phenocrysts (up to 5 mm in length) and composes less than 7 percent of the rock. Apatite, quartz, and magnetite occur as inclusions in the plagioclase and K feldspar.

Mineralized dikes are pervasively altered and contain abundant argillized feldspar and biotitized amphibole phenocrysts in an aphanitic groundmass. A small proportion of primary biotite is also present. The prealteration modal mineralogy of these mineralized dikes is estimated to have been 32 percent plagioclase, 30 percent orthoclase, 25 percent quartz, and 14 percent ferromagnesian and accessory minerals.

Alteration and Mineralization

Hydrothermal alteration and mineralization at Sungun are centered on the stock and were broadly synchronous with its emplacement (Figs. 3, 4, and 5). Early hydrothermal alteration was dominantly potassic and propylitic and was followed by later phyllic, silicic, and argillic alteration.

Potassic alteration

The earliest alteration is represented by potassic mineral assemblages developed pervasively and as halos around veins in the deep and central parts of the Sungun stock (Figs. 3, 4, and 5). Potassic alteration is characterized by K feldspar, irregularly shaped crystals of Mg-enriched biotite, and anhydrite. This alteration displays a close spatial association with mineralization; perhaps as much as 80 percent of the copper and all the molybdenum were emplaced during this alteration episode. On average, potassically altered rocks contain 28 percent plagioclase, 35 percent orthoclase (2 mm to 2 cm in diam), 20 percent quartz, 15 percent ferromagnesian minerals (mainly biotite, and sericite and chlorite after biotite), and 2 percent chalcopyrite, pyrite, titanite, zircon, scheelite, urani-

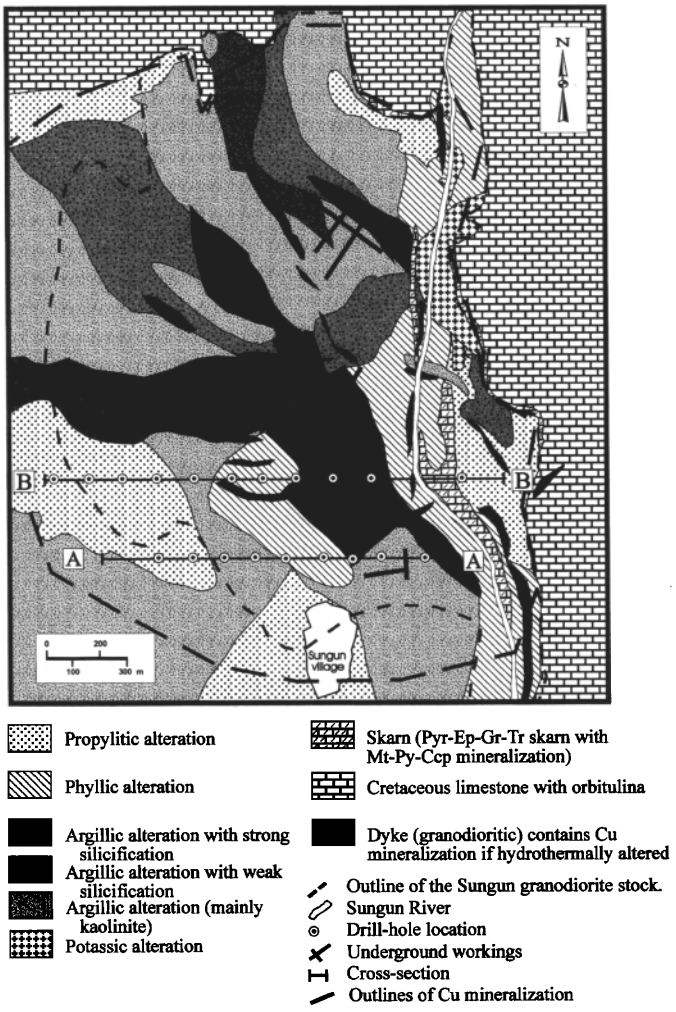

FIG. 3. Detailed alteration map of the Sungun deposit (modified from an unpublished preliminary alteration map prepared by the Ahar Copper Company).

nite, bismuthinite, and rutile. Petrographic observations and electron microprobe analyses indicate the presence of two compositionally distinguishable types of biotite within this alteration zone: primary biotite, which is Fe enriched, brown in color, and generally euhedral; and hydrothermal biotite, which is mainly pale brown to greenish-brown in color, very ragged, and Mg enriched (Table 1). The hydrothermal biotite is generally interstitial to feldspar and quartz, and locally replaced hornblende and primary biotite phenocrysts. Electron microprobe data indicate that some grains of potassium feldspar are rimmed by albite (An_{1-4}), suggesting a later transition alteration event. Magnetite is rarely present, except in skarns. Relict crystals of secondary biotite are observed almost everywhere in the stock, suggesting that potassic alteration was initially very extensive but has been subsequently overprinted and obliterated by later stages of alteration.

Quantitative study of whole-rock chemical data indicates that the principal mass changes accompanying potassic alteration were an appreciable addition of K, a small addition of Si, and large depletions of calcium and magnesium. These reflect the replacement of plagioclase and amphibole by K feldspar and biotite, respectively (Hezarkhani, 1997).

Propylitic alteration

There is a relatively sharp boundary between the propylitic and potassic alteration zones in the deep part of the deposit, but at shallow levels this contact is obscured by later phyllic alteration (Figs. 4 and 5). Propylitic alteration is pervasive and represented mainly by chloritization of primary and secondary biotite and groundmass material in rocks peripheral to the central potassic zone. Epidote replaced plagioclase, but this alteration is less pervasive and intense than chloritization. Electron microprobe analyses indicate that the chlorite composition corresponds mostly to that of clinochlore and pycnochlorite. Minor minerals associated with propylitic alteration are albite, calcite, sericite, anhydrite (gypsum), and pyrite.

Transition zone alteration

Potassic alteration is overprinted by a large zone of pervasive transition alteration in the central part of the stock, which grades upward into phyllic alteration. Transition alteration is characterized by albite replacement of more An-rich plagioclase and by albite rims on orthoclase. Minor sericite and pyrite also partially replaced plagioclase, biotite, and hornblende. A distinguishing characteristic of this type of alteration is the white color of the affected rocks. This change of color from the original gray to white reflects a strong depletion of ferromagnesian minerals like hornblende and biotite. In contrast to potassic alteration, K was depleted and Ca added, probably due to breakdown of K feldspar and addition of anhydrite, respectively. Other major elements were relatively unchanged. The most important change among trace elements was the depletion in Cu (Hezarkhani, 1997).

Phyllic alteration

The change from transition alteration to phyllic alteration is gradual and is marked by an increase in the proportion of muscovite. It is difficult to separate transition and phyllic alteration because of intense silicification during the latter alteration. Phyllic alteration is characterized by the replacement of almost all rock-forming silicates by sericite and quartz, and overprints the earlier formed potassic and transition zones. Pyrite forms up to 5 vol percent of the rock and occurs in veins and disseminations. Quartz veins are surrounded by weak sericitic halos. Vein-hosted pyrite is partially replaced by chalcopyrite. Silicification was synchronous with phyllic alteration and variably affected much of the stock and most dikes. This observation is supported by whole-rock chemical analyses, which show that Si was added in higher proportions than for any other stage of the alteration (Hezarkhani, 1997). The rocks were depleted in other major elements, except Al and Mg, to varying degrees. Finally, in contrast to the transition zone, appreciable Cu was added to the rock during phyllic alteration.

Argillic alteration

Feldspar is locally altered to clay down to a depth of 400 m, and within 80 m of the erosional surface the entire rock has been altered to an assemblage of clay minerals, hematite,

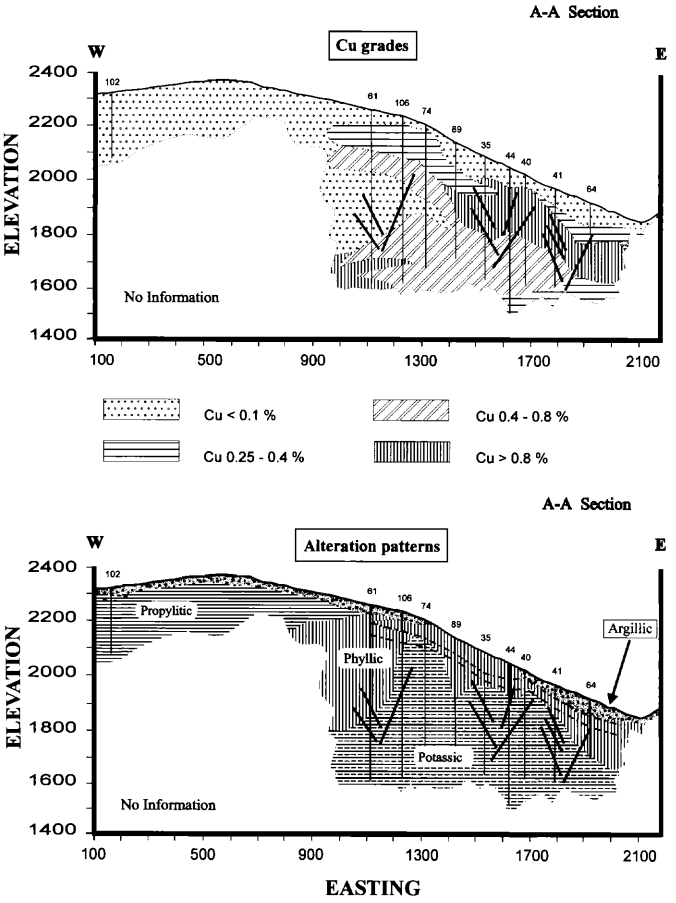

FIG. 4. Profiles showing the distribution of Cu grades and alteration assemblages along cross section A-A. Numbers on surface indicate drill holes. The thick lines represent dikes. The thin dashed and dot-dashed lines indicate the base of the oxide and supergene zones, respectively.

and quartz. The affected rocks are soft and white colored. XRD analyses indicate that kaolinite is the dominant phyllosilicate and that it is accompanied by illite. The shallow alteration is interpreted to represent a supergene blanket over the deposit and the deeper clay alteration of feldspar may have had the same origin. However, the possibility cannot be excluded that the latter represents an argillic stage of the hypogene alteration.

Mineralization

Hypogene copper mineralization was introduced during potassic alteration, and to a lesser extent during phyllic alteration, and exists as disseminations and in veinlet form. During potassic alteration, the copper was deposited as chalcopyrite and minor bornite; later hypogene copper was deposited mainly as chalcopyrite. Hypogene molybdenite was concentrated mainly in the deep part of the stock and is associated exclusively with potassic alteration, where it is found in quartz veins accompanied by K feldspar, anhydrite, sericite, and lesser chalcopyrite (see section on vein classification). The concentration of sulfides and copper mineralization increases outward from the central part of the stock, with the latter generally reaching a maximum of >0.8 wt percent along the interface between the potassic and phyllic alteration zones and in silicified phyllically altered rocks (Figs. 4 and 5); sulfide concentrations, mainly pyrite, are highest in the phyllic alteration zone. The ratio of pyrite to chalcopyrite increases from 4:1 in the outer parts of the potassic alteration zone to 15:1 toward the margins of the stock.

At the exposed surface of the deposit, rocks are highly altered and the only mineral which has survived supergene argillization is quartz. Most of the sulfide minerals have been leached, and copper was concentrated in an underlying supergene zone by downward-percolating ground waters. This zone is very limited and consists of a thin (up to 45 m) blanket containing covellite, chalcocite, and digenite located below a thin, intensely oxidized cap.

Vein Classification

The Sungun deposit contains a well-developed stockwork that is concentrated in the potassic and transition zones (the transition zone is actually the outermost part of the potassic zone and is characterized by a low content of biotite and abundant sericite). On the basis of mineralogy and crosscutting relationships, it is possible to distinguish four main groups of veins representing four episodes of vein formation (Fig. 6): (I) quartz + molybdenite + anhydrite ± K feldspar with sporadic pyrite, chalcopyrite, and bornite; (II) quartz +

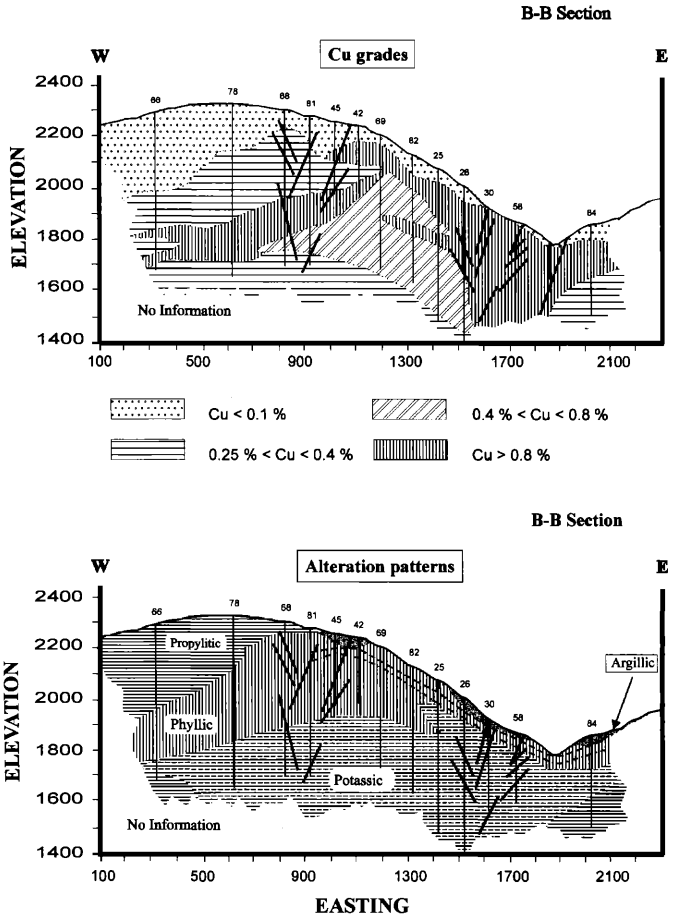

FIG. 5. Profiles showing the distribution of Cu grades and alteration assemblages along cross section B-B. Numbers on the surface indicate drill holes. The thick lines represent dikes. The thin dashed and dot-dashed lines indicate the base of the oxide and supergene zones, respectively

chalcopyrite + pyrite ± molybdenite; (III) quartz + pyrite + calcite ± chalcopyrite ± anhydrite (gypsum) ± molybdenite; and (IV) quartz, and/or calcite, and/or gypsum ± pyrite.

In order to determine the volume percent of each vein type in the different alteration zones, we have used the two-dimensional method of Haynes (1984). First, we split the core (drill core 25) along its axis to expose a rectangular surface of dimension $2r \times T$, where r is the radius of the core, and T is the total length of split core. The density of all veins in a given core was measured by the sum of the lengths of veins which had been exposed in the cut area divided by the area. The length of the fracture is a function of the radius of the core and the angle with which the fracture intersects the core; the area of the rectangle is $2rT$ (Haynes, 1984).

The stockwork system is dominated by group IV and group I veins (up to 21 and 24% by volume of the rock, respectively). Group II and group III veins occupy up to 15 vol percent and 13 vol percent of the rock, respectively. The proportion of the rock occupied by all types of veins averages ~16 vol percent. Group I and II veins occur predominantly in the potassic alteration zone and are also the most important vein groups in the transition alteration zone (Fig. 6). Group III and IV veins are dominant in the phyllic and argillic alteration zones, respectively.

Group I veins

Group I veins are discontinuous, vary in thickness between 0.5 and 3 mm, and formed during the early fracturing of the porphyry stock. Molybdenite is the most important sulfide mineral and occurs mainly along vein margins; K feldspar, anhydrite, chalcopyrite, bornite, and pyrite occur in the central part of the vein, and less commonly, at the margins. There are some traces of bismuthinite (Bi_2S_3) in the molybdenite grains (Fig. 7a). Pyrite and chalcopyrite partially replace the molybdenite. Quartz makes up from 60 to 95 percent of the volume of the veins. The veins are surrounded by potassic, and less commonly, phyllic and propylitic alteration halos.

Group II veins

Group II veins generally crosscut and in places offset the group I veins. The most important characteristics of group II veins are well-developed sericitic alteration halos and the lack of K feldspar. The volume ratio of chalcopyrite to pyrite is 2:1. Molybdenite contents vary from traces to less than 5 vol percent of the vein. The alteration halos are most obvious in the potassic alteration zone, where hydrothermal biotite in the halo was destroyed. The sericitic alteration halos have thicknesses varying between 1 and 5 mm. Vein quartz is relatively coarse grained and tends to be oriented perpendicular to the walls of the vein. Sulfide minerals are located mainly in a narrow discontinuous layer in the vein centers, but in some cases the sulfides are disseminated through the quartz. Group II veins occur in all alteration zones but are concentrated mainly in the potassic alteration zone. Their thickness varies from 3 to 30 mm, and they are generally more continuous than group I veins.

Group III veins

Group III veins crosscut both group I and II veins and in some cases offset the earlier formed veins. Group III veins are most abundant in the phyllic alteration zone and are relatively continuous, commonly layered, and vary in thickness from 3 to 50 mm. Quartz occurs mainly near the vein margins with anhydrite, calcite, and sulfide minerals intergrown in the vein centers. Quartz is relatively coarse grained, and locally shows optical zoning (overgrowths). The only copper mineral is chalcopyrite, which is observed mainly as small blebs and inclusions in pyrite. Early formed anhedral to subhedral grains of pyrite are replaced by anhedral grains of chalcopyrite (Fig. 7b and c). Group II and III veins appear to have a common origin, with group III veins probably having formed by reopening of group II veins. As will be discussed in the section on fluid inclusions, primary saline fluid inclusions similar to those in group II veins, are present in the centers of zoned quartz crystals in group III veins. The paucity of chalcopyrite and other copper minerals in group III veins suggests that they have been leached by later fluid circulating in these veins.

Group IV veins

Group IV veins crosscut all the other vein groups and represent the youngest vein-forming event in the Sungun stock.

TABLE 1. Composition of Magmatic and Hydrothermal Biotite in the Sungun Porphyry Copper Deposit

	Hydrothermal biotite (greenish-brown color)					Magmatic biotite (dark brown color)				
Sample no.	25-431	25-431	25-431	25-431	34-477	25-514	34-477	34-163	34-164	34-163
Drill core	25	25	25	25	34	25	34	34	34	34
Type[1]	K	K	K	K	Phc	Frs	Phc	Trn	K	Trn
SiO_2 (wt %)	41.29	39.25	39.03	38.74	41.29	38.58	37.27	37.60	38.58	37.27
TiO_2	2.02	2.17	2.11	3.91	2.02	3.82	4.27	4.95	3.82	4.27
Al_2O_3	15.05	15.50	15.54	15.53	15.05	14.55	13.53	22.86	14.55	13.53
FeO[2]	2.53	4.17	4.18	4.79	2.53	15.69	16.38	13.51	15.69	16.38
MnO	0.00	0.04	0.01	0.02	0.00	0.17	0.18	0.06	0.17	0.18
MgO	23.18	21.50	21.58	21.39	23.18	14.34	14.40	14.39	14.34	14.40
CaO	0.00	0.00	0.04	0.04	0.00	0.03	0.01	0.13	0.03	0.01
Na_2O	0.14	0.18	0.17	0.20	0.14	0.30	0.30	0.09	0.30	0.30
K_2O	10.51	10.43	10.25	10.34	10.51	9.35	9.41	2.26	9.35	9.41
F	2.60	1.96	2.10	1.87	2.60	0.38	0.33	0.38	0.38	0.33
Cl	0.04	0.09	0.08	0.07	0.04	0.20	0.17	0.05	0.20	0.17
Total	97.35	95.29	95.09	96.91	97.35	97.41	96.24	96.29	97.41	96.24
Number of atoms based on 11 O										
Si	2.77	2.75	2.72	2.68	2.77	2.81	2.77	2.72	2.81	2.77
Ti	0.10	0.11	0.11	0.20	0.10	0.21	0.24	0.05	0.21	0.24
Al	1.20	1.28	1.29	1.27	1.20	1.26	1.20	2.02	1.26	1.20
Fe	0.14	0.24	0.24	0.28	0.14	0.96	1.02	0.84	0.96	1.02
Mn	0.00	0.00	0.00	0.00	0.00	0.01	0.01	0.00	0.01	0.01
Mg	2.32	2.23	2.24	2.20	2.32	1.56	1.60	1.37	1.56	1.60
Ca	0.00	0.00	0.00	0.00	0.00	0.00	0.00	0.01	0.00	0.00
Na	0.02	0.02	0.02	0.03	0.02	0.04	0.04	0.01	0.04	0.04
K	0.90	0.93	0.91	0.91	0.90	0.90	0.89	0.21	0.87	0.89
F	0.55	0.43	0.46	0.41	0.55	0.09	0.08	0.09	0.09	0.08
Cl	0.00	0.01	0.01	0.01	0.00	0.02	0.02	0.01	0.02	0.02
F/(F + Cl)	1.00	0.98	0.98	0.98	1.00	0.82	0.80	0.90	0.82	0.80
Fe/(Fe + Mg)	0.06	0.10	0.10	0.11	0.06	0.38	0.39	0.38	0.38	0.39

[1] Frs = fresh rock, K = potassic zone, Phc = phyllic zone, Trn = transition zone
[2] FeO = total Fe

They are very thick (up to 17 cm) and are filled by quartz, and/or calcite, and/or gypsum. Group IV veins are found mainly in the propylitic zone, but also occur locally in the phyllic and potassic alteration zones. The only sulfide mineral is pyrite, which occupies ~10 vol percent of these veins. Group IV veins are usually surrounded by zones of silicification up to 3 cm wide.

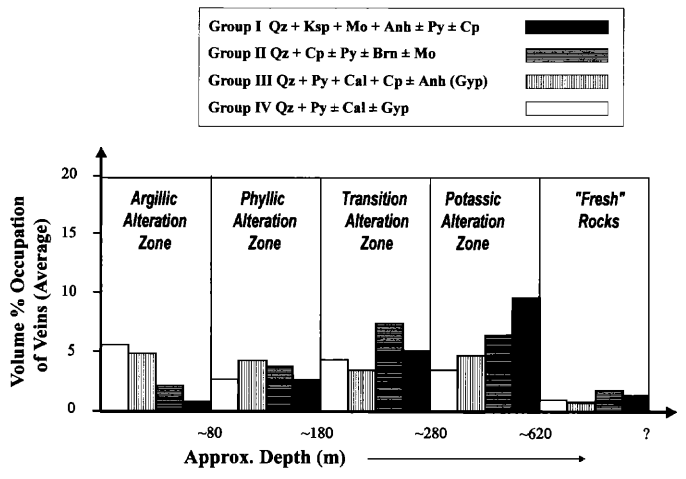

FIG. 6. Diagram showing the volume proportions of the different vein groups in each of the alteration zones.

Fluid Inclusion Studies

Fluid inclusions are abundant in quartz of all the vein types and range in diameter from 1 up to 15 μm. The majority of inclusions examined during this study had diameters of 4 to 12 μm. They are also common in quartz phenocrysts, but are too small (<3 μm) to be analyzed microthermometrically. Most of our measurements were conducted on fluid inclusions in group I and II veins, with a few from group III veins. Group IV veins do not contain any workable fluid inclusions.

Fluid inclusion classification

Fluid inclusions were classified into three main types based on the number, nature, and proportion of phases at room temperature.

LV inclusions consist of liquid + vapor ± solid phases, with the liquid phase volumetrically dominant. These fluid inclusions are common in all mineralized quartz veins and are abundant in group II and III veins. Their diameters range from 3 to 12 μm. Vapor bubbles are variable in size but constitute less than 35 percent of inclusion volumes. The inclusions homogenize to liquid. In a small number of LV fluid inclusions, a cube of halite (<1 μm in diameter) and

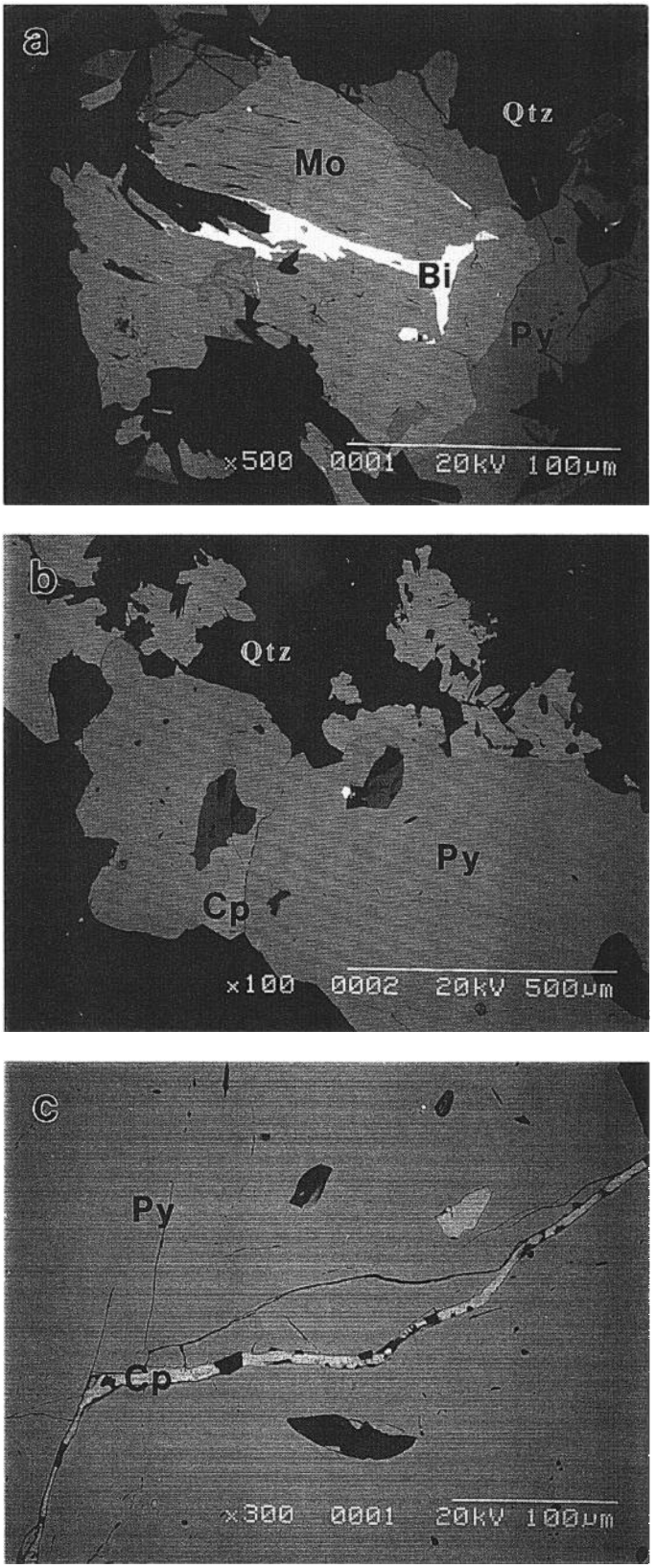

FIG. 7. Scanning electron photomicrographs. (a). Molybdenite with associated anhedral bismuthinite and pyrite. (b). Pyrite altered to chalcopyrite. (c). Chalcopyrite filling fractures in pyrite. Abbreviations: Bi = bismuthinite, Cp = chalcopyrite, Mo = molybdenite, Py = pyrite, Qtz = quartz.

unidentified transparent or opaque minerals (mainly hematite) were observed. The distribution and volume of solid phases are irregular (<5 to >10%), suggesting that they represent trapped solids rather than daughter minerals.

VL inclusions contain vapor + liquid ± solid phases. Vapor bubbles are variable in size, but in all cases consist of >60 percent of the inclusion volume. These inclusions mainly homogenize to vapor, rarely to liquid, or by critical behavior. Most VL inclusions contain only vapor + liquid. However, some inclusions contain a single solid phase which is either halite or an unidentified mineral, probably also trapped.

LVHS inclusions are multiphase and consist of liquid + vapor + halite + other solids. Based on the number and type of the solids, we have further classified LVHS fluid inclusions into three subtypes. Subtype S_1 inclusions are characterized by the presence of halite + chalcopyrite ± anhydrite ± a K-Fe-Cl phase (identification of this mineral is discussed below). Halite, anhydrite, and chalcopyrite have consistent phase ratios and are interpreted to be daughter minerals. Vapor bubbles occupy <25 percent of the inclusion by volume. Subtype S_2 inclusions contain sylvite in addition to the phases in S_1 inclusions. The solid phases occupy ~60 percent of inclusion volumes, and the vapor bubbles ~20 percent. Subtype S_3 inclusions contain halite, which is commonly accompanied by hematite, but they do not contain chalcopyrite, sylvite, and the K-Fe-Cl phase. The volume of the solid phases is typically <40 percent of the inclusions and the bubble volumes range between 20 and 60 percent.

Solid phases in fluid inclusions

Halite and sylvite in the inclusions were identified by their cubic and subcubic shapes and optical isotropy. The identification was confirmed by SEM-EDAX analyses which yielded peaks for Na/Cl and K/Cl, respectively. Sylvite was distinguished from halite by its rounded edges and lower relief; it also dissolves at lower temperatures. Halite crystals are generally larger and more common than those of sylvite and have a well defined habit. Chalcopyrite was identified on the basis of its optical characteristics (opacity and triangular cross section) and composition in opened inclusions (SEM-EDAX analyses yielded peaks for Cu, Fe, and S). Anhydrite forms transparent anisotropic prisms (Fig. 8a) and was shown by SEM-EDAX analyses to consist only of Ca and S (elements lighter than F could not be analyzed). Hematite was easily identified from its red color, hexagonal shape, extremely high index of refraction, and high birefringence (this identification was confirmed by SEM-EDAX analyses on opened inclusions, which only produced a peak for Fe). A transparent, colorless to pale green solid with a rounded shape and strong birefringence, which dissolves at ~200°C, was shown by SEM-EDAX analyses to consist of K, Fe, and Cl. This solid could be the K-Fe chloride, erythrosiderite ($K_2FeCl_5 \cdot X_{H_2O}$).

Distribution of fluid inclusions types

The Sungun intrusions have undergone repeated episodes of fracturing and healing, with multiple generations of fluid inclusions representing the evolution of hydrothermal fluids and corresponding alteration and mineralization.

LV inclusions are found in all vein groups but occur in variable proportions. They are most abundant in the group

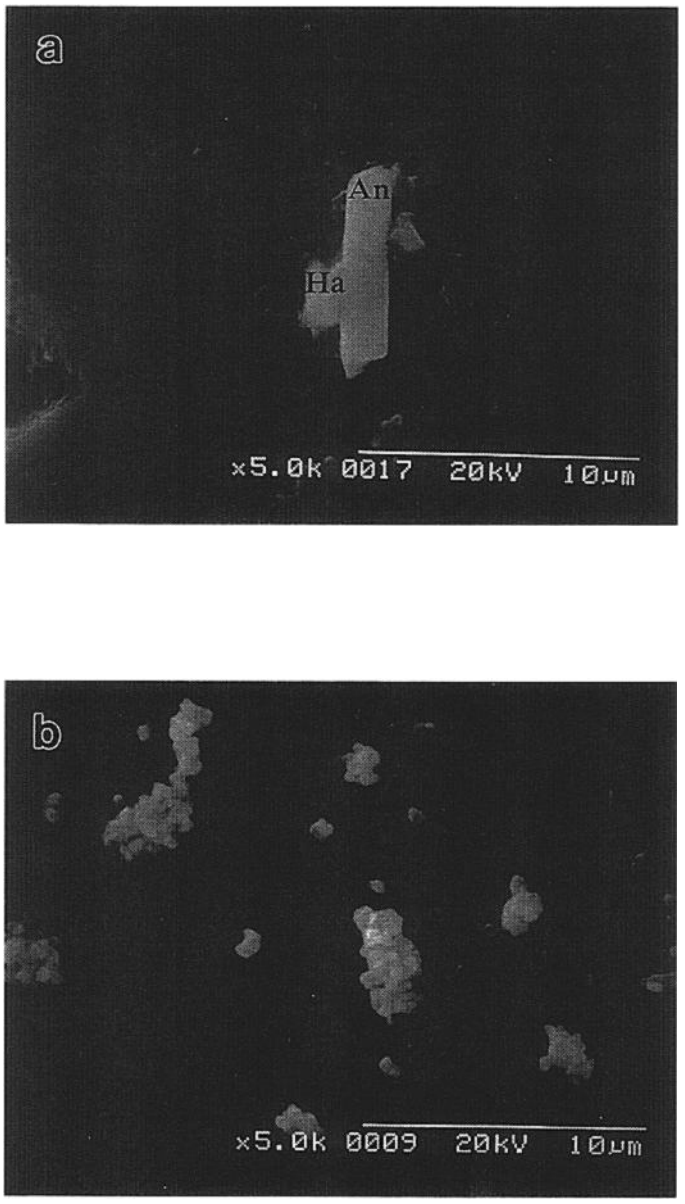

FIG. 8. Scanning electron photomicrographs of daughter minerals from decrepitated quartz-hosted fluid inclusions. (a). Group II quartz veins; An = anhydrite and Ha = halite. (b). Group I quartz veins; accumulations of both halite and sylvite crystals.

II and III veins and are rare in group I veins. Most LV inclusions are distributed along healed fractures and are secondary.

VL inclusions are found in quartz phenocrysts from fresh rocks and in group I, II, and III quartz veins. Some of these inclusions occur in growth zones in group I and II quartz veins, where they are accompanied by LVHS fluid inclusions, indicating that at least some of them are primary. VL inclusions are generally elongate and have rounded ends, but some have negative crystal shapes. Some of the VL inclusions have variable liquid-vapor ratios and may have formed from the necking-down of LVHS inclusions or heterogeneous entrapment of liquid and vapor.

LVHS inclusions up to 10 μm in diameter are found in all veins, from the deepest, potassically altered part of the stock (group I and II veins) through to the shallow-level veins. At shallow levels (group III veins), most of the LVHS inclusions are of subtype S_3, but at deeper levels (mainly group I and II veins), subtypes S_1 and S_2 predominate. Up to seven solid phases have been observed in a single LVHS inclusion. The coexistence of LVHS inclusions (mainly $LVHS_1$ and $LVHS_3$) and vapor-rich inclusions with consistent phase ratios in the growth zones of quartz grains from potassic and phyllic alteration zones suggests a primary origin and coexistence of two immiscible aqueous fluids.

Fluid inclusion population I: $LVHS_1$, $LVHS_2$, and VL fluid inclusions occur in group I and II quartz veins from the potassically altered zone (35–500 m below the present erosional surface), but are rare at shallow levels in the phyllic alteration zone. In group I veins, $LVHS_1$ and $LVHS_2$ fluid inclusions commonly form isolated clusters in the cores of quartz grains. VL inclusions commonly occur along microfractures, but they are also present in clusters with $LVHS_1$ fluid inclusions. $LVHS_1$, $LVHS_2$, and VL fluid inclusions, which have been identified in quartz from group II and III veins in phyllic alteration zones at shallow levels, may be relics of earlier potassic alteration. These three fluid inclusion types are interpreted to represent the earliest episode of fluid entrapment in the deposit.

Fluid inclusion population II: At shallower levels, in the phyllic alteration zone, there is a close spatial association of solid-rich $LVHS_3$ and VL fluid inclusions. They are found together in growth zones but occur mainly along healed fractures. This population of inclusions is spatially associated with LV inclusions, especially in group III veins, although clearly the latter must have been trapped separately from the $LVHS_3$ inclusions, if, as discussed later, halite is a daughter mineral. The relative timing of entrapment of the two inclusion types is unclear.

Fluid inclusion population III: LV fluid inclusions occur in all vein groups but are most common in group II and III veins from phyllic and propylitic alteration zones. They are clearly located along fracture planes and are secondary in origin. LV inclusions appear to represent a later stage fluid that circulated in the intrusion.

Fluid inclusion microthermometry

Microthermometric studies were carried out on 25 samples of quartz from group I, II, and III veins. Temperatures of phase changes in fluid inclusions were measured with a FLUID, Inc., U.S.G.S.-type gas-flow stage which operates by passing preheated or precooled N_2 gas around the sample (Werre et al., 1979). Stage calibration was performed using synthetic fluid inclusions. Accuracy at the standard reference temperatures was ±0.2°C at −56.6°C (triple point of CO_2), ±0.1°C at 0°C (melting point of ice), ±2°C at 374.1°C (critical homogenization of H_2O), and ±9°C at 573°C (alpha to beta quartz transition). The heating rate was approximately 1°C/min near the temperatures of phase transitions.

Low-temperature phase changes: The temperatures of initial (T_e) and final melting ($T_{m_{ice}}$) of ice were measured on type LV, VL, and LVHS fluid inclusions. In the case of type VL inclusions, T_e was difficult to determine because of the

high vapor/liquid ratios. Clathrate formation was not observed in any of the inclusions, which rules out the presence of significant CO_2. The crushing of quartz under anhydrous glycerine confirmed this conclusion; the vapor bubble collapsed during crushing in all but a few inclusions, and in the latter inclusions, the bubble size was unchanged or increased slightly, indicating that the maximum pressure of incondensible gases was ~1 bar.

The temperatures of initial ice melting (T_e) of most LV fluid inclusions are between −25° and −16°C (Fig. 9), suggesting that NaCl ± KCl are the principal salts in solution. The $T_{m_{ice}}$ values for these inclusions range from −1° to −10°C (Fig. 10), corresponding to salinities of 1.7 to 14 wt percent NaCl equiv, respectively (Sterner et al., 1988). A small proportion of LV inclusions in quartz phenocrysts in shallow dikes have T_e between −25° and −39°C, suggesting the presence of appreciable $CaCl_2$, $FeCl_2$, or $MgCl_2$ in addition to NaCl and KCl. The $T_{m_{ice}}$ values for LV fluid inclusions in group I quartz veins range from −1.3° to −8.1°C, corresponding to a salinity of 2.3 to 9.6 wt percent NaCl equiv (Sterner et al., 1988); in group II quartz veins they range from −1.2° to −10.5°C, corresponding to a salinity from 2.1 to 14.5 wt percent NaCl equiv; and in group III quartz veins they range from −2.1 to −12.3°C corresponding to a salinity from 3.5 to 16.3 wt percent NaCl equiv (Table 2). The salinity data discussed above ignore a small number of LV inclusions which contain cubes of halite that are interpreted to have been entrapped with the fluid.

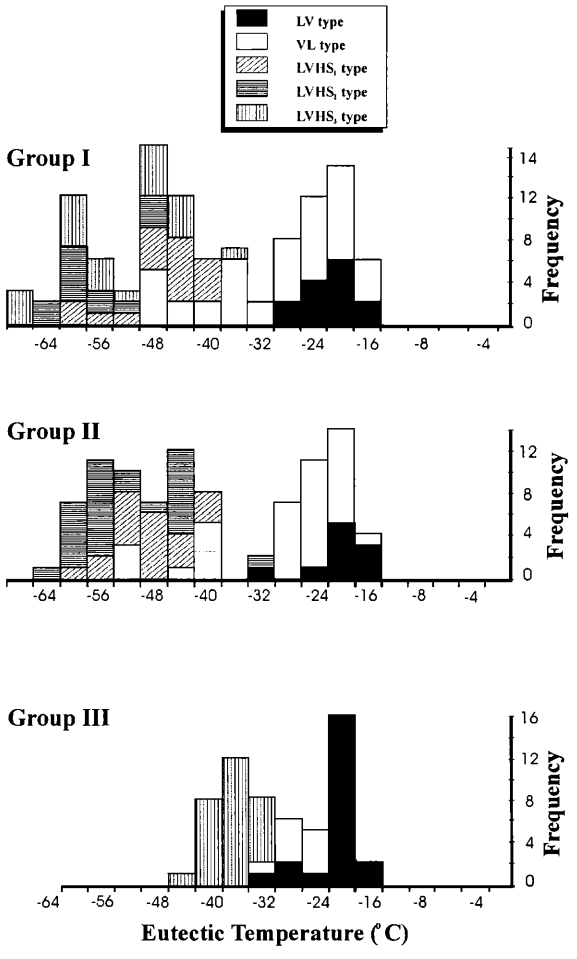

FIG. 9. Histograms of eutectic temperatures for LV, VL, and LVHS fluid inclusions from mineralized quartz veins.

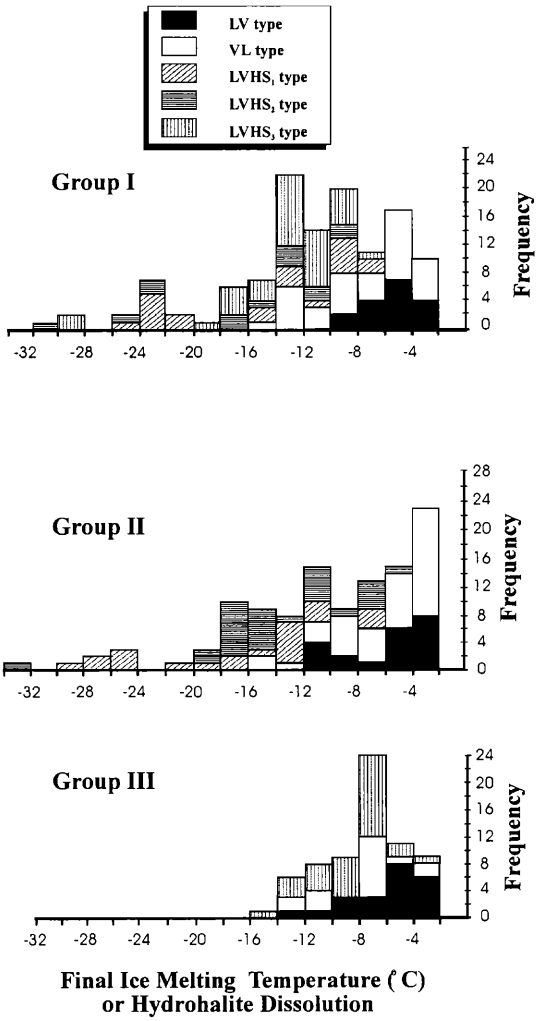

FIG. 10. Histograms of final ice melting and hydrohalite dissolution temperatures for fluid inclusions from mineralized quartz veins.

The T_e values of VL fluid inclusions range from −48° to −18°C with a mode of ca. −26°C, suggesting that Na and K are the dominant cations in the solution but that there are significant concentrations of divalent cations. The $T_{m_{ice}}$ value for these inclusions varies from −0.5° to −14.9°C, which corresponds to a salinity between 0.8 and 18.5 wt percent NaCl equiv. The low T_e (−31° to −46°C) for some of the VL inclusions in group I and II veins could indicate that these inclusions are the product of necking down of LVHS inclusions or heterogeneous entrapment (see below).

Owing to the small volume of liquid in LVHS fluid inclusions, it is difficult to measure T_e and the melting temperature of hydrohalite ($T_{m_{HH}}$). The eutectic temperatures that could be measured in group I and II veins ($LVHS_1$ and $LVHS_2$) range from −30° to −64.4°C, suggesting important concentrations of Fe, Mg, Ca, and/or other components in addition

TABLE 2. Fluid Inclusion Microthemometric Data

Sample no.[1]	Stage[2]	Origin[3]	Type[4]	T_e (°C) range	Avg	$T_{m_{ice}}$ (°C) range	Avg	$T_{m_{HH}}$ (°C) range	Avg	$T_{m_{halite}}$ (°C) range	Avg	$T_{m_{sylvite}}$ (°C) range	Avg	$T_{h_{L-V}}$ (°C) range	Avg	Salinity range	Avg
106-627	I	P	VL	−19.7 to −27.3 (5)	−24.7	−4.7 to −11.5 (5)	−7.7							583.0 to 433.0 (5)	506.6	15.5 to 7.4 (5)	11.1
106-627	I	S	LV	−23.0 to −26.2 (5)	−24.4	−2.1 to −5.3 (5)	−3.8							287.0 to 249.0 (5)	273.6	8.3 to 3.5 (5)	6.0
34-372	I	P	$LVHS_1$	−42.5 to −63.0 (9)	−51.2	−6.4 to 25.0 (9)	−13.9	9.8 to 6.3 (3)	8.0	453.0 to 331.0 (9)	379.5			372.0 to 273.5 (9)	300.4	53.6 to 41.0 (9)	45.5
25-421	I	P	$LVHS_2$	−44.0 to −63.0 (5)	−54.3	−10.3 to −22.0 (5)	−15.8	5.0 to 7.0 (2)	6.0	456.0 to 300.0 (5)	372.7	60.5 to 90.1 (5)	76.7	364.0 to 487.0 (5)	407.3	38.2 to 54.0 (5)	45.1
34-372	I	P	$LVHS_3$	−41.0 to −59.0 (21)	−50.1	−3.6 to −30.0 (21)	−14.5	13.0 to 5.4 (6)	7.6	283.0 to 450.0 (21)	359.6	79.0 to 73.0 (2)	76	435.0 to 291.0 (21)	338.2	53.3 to 38.0 (21)	43.7
34-372	I	Ps	VL	−20.0 to −48.7 (12)	−32.6	−1.3 to −13.4 (12)	−8.7							620.0 to 383.0 (12)	496.1	2.9 to 16.9 (12)	13.0
25-421	I	S	LV	−16.0 to −29.1 (10)	−23.6	−1.3 to −8.1 (10)	−4.8							437.9 to 255.0 (10)	317.1	2.2 to 11.9 (10)	7.5
25-421	I	S	$LVHS_1$	−63.0 (1)		−13.4 (1)				390.3 (1)				425.0 (1)		46.3 (1)	
25-421	I	S	$LVHS_2$	−51.2 (1)		−8.1 (1)				280.0 (1)		50.3 (1)		395.0 (1)		36.6 (1)	
25-421	I	S	VL	−17.0 to −47.0 (3)	−27.7	−1.1 to −6.8 (3)	−3.1							406.0 to 412.0 (2)	409.0	10.3 to 1.9 (3)	4.8
25-500	I	P	$LVHS_2$	−43.0 to −64.0 (8)	−53.0	−6.4 to −25.2 (8)	−14.1			457.0 to 236.0 (8)	339.1	98.1 to 57.5 (8)	75.8	610.0 to 237.0 (8)	416.4	54.1 to 33.8 (8)	42.1
25-500	I	Ps	$LVHS_1$	−41.3 to −46.3 (2)	−43.8	−8.1 to 10.2 (2)	−9.1			403.0 to 291.0 (2)	347.0			348.3 to 293.0 (2)	320.7	47.8 to 37.5 (2)	42.6
25-500	I	S	LV	−23.2 to −58.0 (2)	−40.6	−7.3 to 9.8 (2)	−8.6			487 (1)				450.0 to 310.8 (2)	380.4	13.8 to 10.9 (2)	12.3
25-466	II	P	$LVHS_1$	−39.2 to −64.9 (8)	−50.6	−5.0 to −21.5 (8)	−11.7			450.0 to 369.0 (8)	410.2			390.0 to 276.0 (8)	310.7	53.3 to 44.2 (8)	48.7
25-466	II	P	$LVHS_2$	−30.4 to −41.0 (2)	−35.7	−3.5 to −6.6 (2)	−5.1			363 to 373.0 (2)	368.0			380.0 to 305.0 (2)	342.5	44.6 to 43.1 (2)	44.1
25-466	II	P	$LVHS_3$	−60.0 to −55.0 (2)	−57.5	−14.0 to −15.0 (2)	−14.5			425.0 to 297.0 (2)	361.0			320 to 277.0 (2)	138.5	50.3 to 37.9 (2)	44.1
25-466	II	Ps	LV	−21.0 to −27.0 (4)	−23.0	−1.2 to −9.7 (4)	−4.2							288.9 to 245.0 (4)	264.7	4.3	
25-466	II	Ps	$LVHS_3$	−54.4 (1)		−13.9 (1)				310.0 (1)				278.0 (1)		38.9 (1)	
25-466	II	S	LV	−48.1 (1)		−8.9 (1)								280.1 (1)		12.8	
25-466	II	S	VL	−31.8 (1)		−2.1 (1)								373.0 (1)		3.5	
25-466	II	S	$LVHS_3$	−45.0 (1)		−15.9 (1)				280.0 (1)				245.0 (1)		36.7	
100-341	II	P	VL	−23.0 to −26.3 (5)	−24.2	−0.6 to −11.7 (5)	−4.1							450.0 to 350.0 (5)	392.8	15.7 to 1.0 (5)	6.0
25-307	II	P	$LVHS_1$	−44.0 to −53.0 (9)	−48.6	−13.0 to −26.0 (9)	−19.4			410.0 to 230.0 (9)	371.0			359.0 to 330.0 (9)	349.7	48.5 to 33.4 (9)	44.8
25-307	II	P	$LVHS_2$	−41.0 to −56.0 (9)	−51.6	−4.9 to −17.5 (9)	−14.1			469.0 to 271.0 (9)	344.2	91.3 to 55.3 (5)	79.8	451.0 to 320.0 (9)	397.6	55.7 to 36.1 (9)	42.8
25-307	II	Ps	VL	−21.6 to −46.0 (3)	−35.6	−0.8 to −7.0 (3)	−4.3							387.2 to 360.0 (3)	373.6	1.4 to 10.5 (3)	6.7
25-307	II	S	VL	−18.0 to −47.0 (27)	−27.8	−1.2 to −12.0 (27)	−8.2							327.0 to 600.0 (27)	421.4	1.4 to 16.0 (27)	8.9
25-478	II	P	LV	−19.0 to −33.5 (6)	−21.9	−1.3 to −4.3 (6)	−2.9							271.0 to 365.7 (6)	300.3	8.0 to 6.7 (6)	4.9
25-478	II	P	$LVHS_1$	−42.2 to −57.0 (5)	−48.3	−9.0 to −28.0 (5)	−15.0	12.2 (1)		216.0 to 395.0 (5)	321.3	75		258 to 342.0 (5)	312.5	32.7 to 46.9 (5)	40.6
25-478	II	P	$LVHS_2$	−41.3 to −54.0 (3)	−48.3	−8.3 to −17.0 (3)	−13.8			446.0 to 291.0 (3)	370.0	98		398.0 to 262.7 (3)	316.6	52.8 to 37.5 (3)	45.0
25-487	II	Ps	LV	−21.0 to −23.1 (2)	−22.1	−5.8 to −7.5 (2)	−6.7							510.0 to 282.7 (2)	396.4	9.0	
25-487	II	Ps	VL	−20.2 to −26.2 (3)	−23.1	−0.5 to 7.2 (3)	−3.6							609.1 to 620.0 (3)	614.5	10.8 to 0.9 (3)	5.6
25-487	II	S	LV	−16.0 to −22.0 (3)	−19.3	−1.5 to −4.1 (3)	−2.6							330.0 to 316.6 (3)	321.4	6.6 to 2.6 (3)	4.3
33-473	II	P	$LVHS_1$	−58.0 (1)		−5.1 (1)				405.0 (1)				278.1 (1)		48.0 (1)	
33-473	II	P	$LVHS_2$	−56.0 to −49.0 (4)	−52.3	−7.1 to −14.9 (4)	−10.1			498.0 to 437.3 (4)	459.8	119.0 to 85.1 (4)	98.3	485.0 to 410.0 (4)	450.8	59.5 to 51.7 (4)	54.6
33-473	II	P	VL	−52.3 (1)		−5.4 (1)				450.1 (1)				427.0 (1)		8.4	
100-341	II	S	$LVHS_3$	−53.2 (1)		−33.3 (1)		11.2 (1)		295.0 (1)				307.0 (1)		37.8 (1)	
106-627	III	Ps	$LVHS_3$	−65.0 (1)		−18.5 (1)				359.1 (1)				215.0 (1)		43.3	
25-233	III	P	VL	−4.2 to −30.6 (6)	−27.5	−7.3 to −14.9 (6)	−10.0							420.0 to 315.0 (6)	361.8	18.6 to 6.7 (6)	13.6
25-233	III	P	LV	−19.0 to −27.5 (17)	−23.2	−1.3 to −12.3 (17)	−6.2							345.0 to 225.0 (17)	296.7	16.3 to 2.2 (17)	9.2
25-273	III	P	$LVHS_3$	−26.0 to −42.1 (20)	−35.3	−4.1 to −9.0 (20)	−7.0			351.0 to 211.0 (20)	261.6			345.0 to 215.0 (20)	275.2	42.5 to 32.7 (20)	35.6
25-273	III	S	$LVHS_3$	−40.3 to −42.0 (3)	−41.1	−6.3 to −12.0 (3)	−9.5			260.0 to 271.1 (3)	263.4			320.0 to 231.0 (3)	265.3	36.1 to 35.3 (3)	35.5
25-280	III	P	LV	−18.5 to −22.0 (5)	−20.4	−2.9 to −7.2 (5)	−5.1							273.0 to 241.0 (5)	257.3	10.8 to 4.8 (5)	7.9
25-280	III	P	VL	−23.5 to −30.6 (9)	−26.3	−1.2 to −13.2 (9)	−7.3							605.0 to 381.0 (9)	469.6	16.6 to 1.6 (9)	10.3
25-280	III	Ps	LV	−19.4 to −22.0 (6)	−21.0	−2.1 to −6.2 (6)	−4.5							269.0 to 230.0 (6)	241.0	9.5 to 3.5 (6)	7.1
25-307	III	P	$LVHS_3$	−38.0 to −62.0 (9)	−48.4	−3.7 to −13.9 (9)	−8.9			500.0 to 430.0 (9)	459.3			363.0 to 350.0 (9)	356.5	59.8 to 50.7 (9)	55.8
100-234	III	Ps	$LVHS_3$	−31.7 to −46.5 (5)	−38.0	−5.6 to −12.1 (5)	−8.4	−19.0 to −24.0 (5)	−21.9	458.0 to 321.2 (4)	375.0			300.0 to 240.0 (4)	262.0	54.3 to 39.8 (5)	45.2
25-421	III	S	$LVHS_3$	−43.8 to −61.0 (3)	−51.6	−6.5 to −12.4 (3)	−8.7			389.0 to 298.0 (3)	350.3			329.0 to 305.0 (3)	301.7	46.3 to 38.0 (3)	42.7
33-473	III	Ps	LV	−55.0 (1)		−10.5 (1)				275.1 (1)				288.0 (1)		14.5	
33-473	III	S	VL	−53.6 (1)		−9.8 (1)				271.0 (1)				287.8 (1)		13.8	

Number of inclusions measured is given in parentheses; T_e = eutectic temperature, $T_{m_{ice}}$ = ice-melting temperature, $T_{m_{HH}}$ = ice-melting temperature for hydrohylite, T_h = homogenization temperature, Avg = average

[1] Numbers before dash identify drill holes and those after the dash indicate the depth

[2] Stage of mineralized quartz veins

[3] Fluid inclusion origin: P = primary, Ps = pseudosecondary, S = secondary

[4] Types of fluid inclusions

to Na and K in this type of inclusion (Fig. 9). Eutectic temperatures for the $CaCl_2$-H_2O, NaCl-$CaCl_2$-H_2O, and $FeCl_3$-H_2O systems are −49.8°, −52°, and −55°C, respectively (Linke, 1965), and could explain the low first melting temperatures observed for some of the LVHS inclusions. $T_{m_{HH}}$ values vary between −5° and −32°C in LVHS inclusions (Fig. 10). SEM-EDAX analyses of the residues of decrepitated fluid inclusions showed that Fe and Ca are more abundant than Mg (discussed later).

LVHS fluid inclusions (subtype $LVHS_3$) in group III vein quartz yielded distinctly different microthermometric data from those of $LVHS_1$ and $LVHS_2$ inclusions in group I and II veins. The eutectic temperatures vary from −29° to −43°C and the hydrohalite melting temperature varies between −2° and −13°C (Fig. 10).

High-temperatures phase changes: LV fluid inclusions homogenize to liquid ($T_{h_{L+V\rightarrow L}}$) at temperatures between 240° and 330°C, with a well-defined mode atT_{h_L} of ~270°C for groups I and II, and 300°C for group III mineralized quartz veins (Fig. 11). Almost all VL inclusions homogenize to vapor

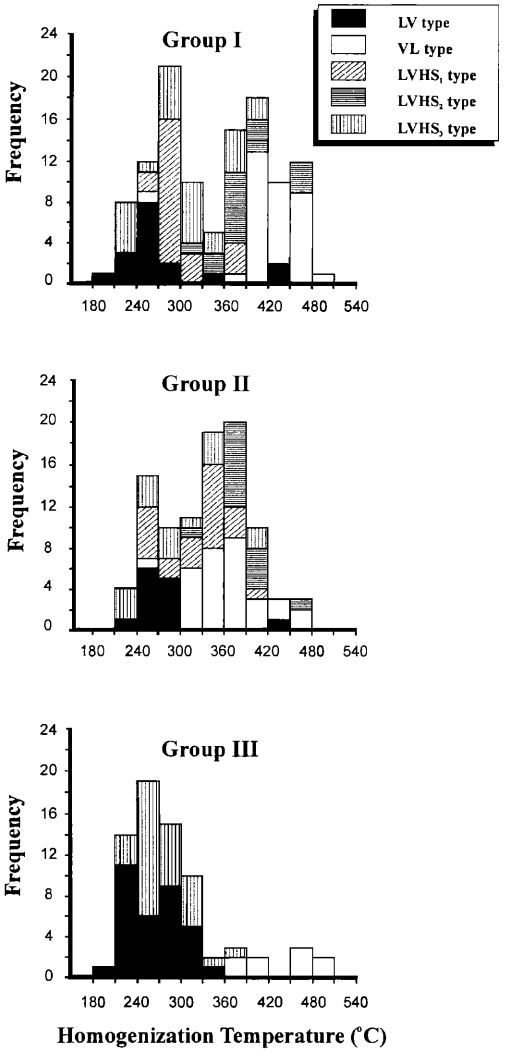

FIG. 11. Histograms of homogenization temperatures for LV, VL, and LVHS fluid inclusions from mineralized quartz veins.

($T_{h_{L+V\rightarrow V}}$) between 320° and 500 °C. VL inclusions from group III veins homogenize at temperatures between 375° and 535°C (Fig. 11), but some of the VL inclusions from group II veins exhibit no changes until the temperature is within ~30°C of the homogenization temperature; the vapor then rapidly expands to fill the inclusion, indicating a near-critical density fluid (cf. Roedder, 1984).

The liquid and vapor phases in $LVHS_1$ and $LVHS_2$ inclusions from group I veins homogenize to liquid at temperatures between ~280° and ~500°C (Fig. 11) and between ~260° and ~460°C in group II veins. The liquid-vapor homogenization temperature for $LVHS_3$ inclusions is from ~220° to ~420°C in group I and II veins and ~220° to ~390°C in group III veins (Fig. 11). The first mineral to dissolve in $LVHS_2$ inclusions is sylvite, at temperatures between 55° and 119°C (group I and II veins). The K-Fe chloride phase ($LVHS_1$ and $LVHS_2$) dissolves between 200° and 256°C, and halite in these inclusions dissolves between 280° and 498°C (group I and II veins). Salinities based on the halite dissolution temperature range from 36 to 60 wt percent NaCl equiv (Sterner et al., 1988; Fig. 12). The halite dissolution temperatures for $LVHS_3$ inclusions are 230° to 450°C in group I and II quartz veins. The halite dissolution temperatures ($T_{m_{halite}}$) in $LVHS_3$ inclusions in group III quartz veins are 198° to 351°C which correspond to salinities of 31 to 42 wt percent NaCl equiv with an average of 34 wt percent NaCl equiv (Table 2).

Most $LVHS_1$ inclusions (group I and II veins) and $LVHS_3$ inclusions in group I and II veins homogenized by vapor disappearance (Fig. 13). By contrast $LVHS_2$ inclusions (group I and II veins) homogenized mainly by halite dissolution. $LVHS_3$ inclusions in group III veins homogenized by other vapor disappearance or halite dissolution (Fig. 13). Anhydrite and chalcopyrite did not dissolve on heating to temperatures in excess of 600°C.

Compositional trends in the system NaCl-KCl-H_2O

The compositions of $LVHS_2$ inclusions, when modeled in the system NaCl-KCl-H_2O, appear to define a linear trend (Fig. 14) similar in many respect to the halite trend of Cloke and Kesler (1979) but directed more strongly toward the H_2O apex than in other porphyry systems (e.g., Eastoe, 1978; Ahmad and Rose, 1980; Wilson et al., 1980). The slope corresponds to a K/Na ratio of approximately 0.26, although it should be cautioned that this provides a very rough estimate of the composition of the fluid as it ignores the possible effects of other ions on the solubility of halite and sylvite. The absence of sylvite in $LVHS_1$ and $LVHS_3$ inclusions is evidence for a K/Na atomic ratio of <0.2 (Roedder, 1984), which is supported by SEM-EDAX analyses on decrepitates from these inclusions (see below).

Decrepitate compositions

Residues from decrepitated fluid inclusions were analyzed using the procedures of Haynes et al. (1988). Ten cleaned, doubly polished thin sections were heated rapidly to a temperature of 450°C, which was sufficient to cause most inclusions to decrepitate and low enough to avoid significant loss of volatile components (Fig. 8a and b). The sections were analyzed using a JEOL JSM-840A scanning electron micro-

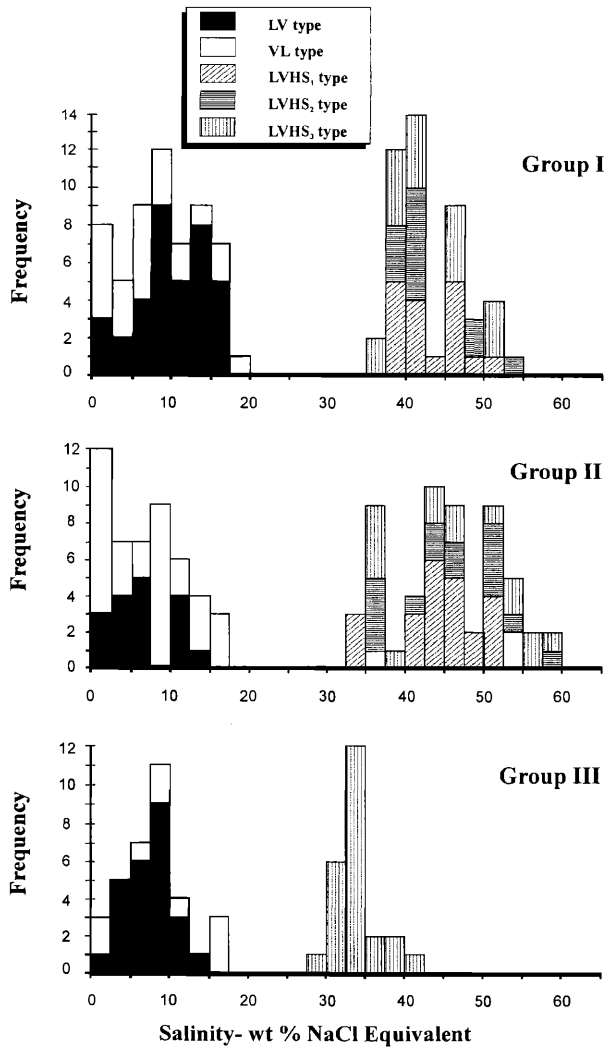

FIG. 12. Histograms of salinities (wt % NaCl equiv) from microthermometric data for LV, VL, and LVHS fluid inclusions in mineralized quartz veins.

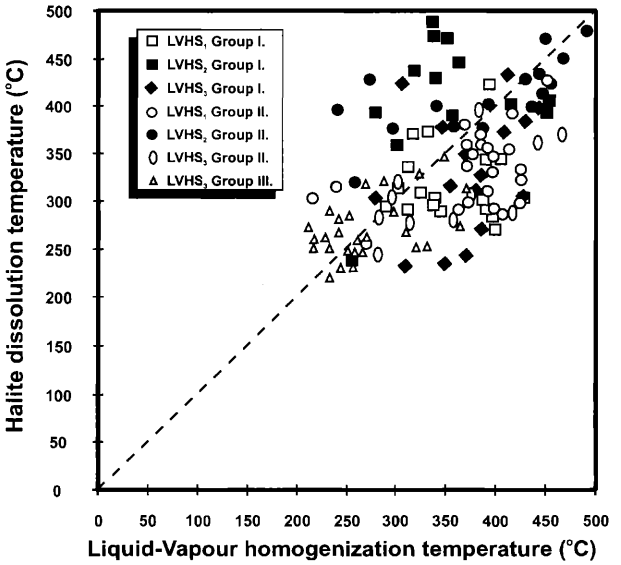

FIG. 13. Liquid-vapor homogenization temperature vs. halite dissolution temperature for halite-bearing fluid inclusions (all LVHS inclusions) in mineralized quartz veins.

scope equipped with a Tracor Northern energy dispersive X-ray spectrometer in raster mode. Analyses in which the sum of cation charges differed by <15 percent from the sum of anion charges were considered reliable and are reported in Table 3.

The following elements were present in appreciable concentrations in the residues: Na, Ca, K, Fe, Mg, Cl, and S. Only Cl, however, was consistent in its concentrations among the various residues analyzed. Other elements varied by at least a factor of two (e.g., Na), and in some cases (e.g., Ca), ranged from 0 to >20 wt percent. Copper is present only in residues from $LVHS_2$ inclusions. In general Na^+ is the dominant cation in residues from all three solid-bearing inclusion types. However, in $LVHS_3$ decrepitates, the atomic proportion of Ca^{2+} approaches and in some cases exceeds that of Na^+. Next to Na^+, Ca^{2+} is the most important cation in $LVHS_1$ inclusions and has high but variable concentrations in $LVHS_2$ inclusions. The concentration of K^+, as expected, is highest in $LVHS_2$ inclusions and among the other cations is exceeded only by that of Na^+. In these inclusions the K/Na ratio ranges from 0.18 to 0.73 and has a mean value of 0.36; the K/Na ratio determined microthermometrically from the dissolution of sylvite and halite ranges between 0.19 and 0.35 (see earlier discussion). The K/Na ratios of $LVHS_1$ and $LVHS_3$ inclusions are 0.03 to 0.15 and 0.07 to 0.24, respectively.

The molalities of the above elements were calculated with the aid of microthermometrically estimated salinities and are presented in Table 3. Of particular interest is the unusually high molality of S, which varied from 0.35 to 0.44 in $LVHS_1$, 0.15 to 2.18 in $LVHS_2$, and 1.25 to 2.41 in $LVHS_3$ inclusions. Some of the high S molalities may reflect contamination with anhydrite. However, even inclusions with little or no Ca con-

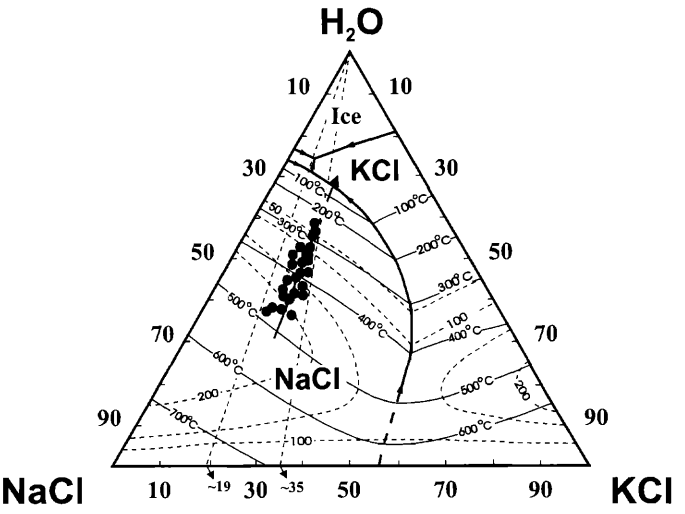

FIG. 14. An NaCl-KCl-H_2O phase diagram showing the compositions of $LVHS_2$ fluid inclusions determined from the dissolution of halite and sylvite (phase diagram after Roedder, 1984).

TABLE 3. Composition of Decrepitate Residues from Different Types of Fluid Inclusions (SEM-EDAX)

No.	Type	Ca	Na	K	Fe	Mg	Al	Cl	S	Mn	Cu	ΣZ^+	ΣZ^-	$\Sigma Z^+ - \Sigma Z^-$	K/Na ratio
							Weight percent								
1	$LVHS_1$	0.54	12.89	0.40	20.85	0.00	0.31	62.19	1.41	1.40	0.00	18.03	−18.42	−0.39	0.03
2	$LVHS_1$	8.25	18.95	0.92	0.98	1.82	1.79	65.69	1.39	0.21	0.00	16.69	−19.40	−2.71	0.05
3	$LVHS_1$	8.25	20.95	3.11	0.98	1.82	1.60	61.69	1.39	0.21	0.00	17.91	−18.27	−0.36	0.15
4	$LVHS_2$	2.83	21.26	9.34	3.15	1.80	0.00	60.37	1.25	0.00	0.00	16.22	−17.81	−1.59	0.44
5	$LVHS_2$	1.24	16.46	11.99	3.70	2.21	1.58	60.62	1.11	1.09	0.00	16.81	−17.79	−0.99	0.73
6	$LVHS_2$	0.83	25.36	6.59	2.83	1.80	1.50	59.11	1.98	0.00	0.00	17.80	−17.91	−0.11	0.26
7	$LVHS_2$	0.00	24.11	4.43	5.08	3.62	0.00	60.51	2.11	0.00	0.14	17.35	−18.38	−1.03	0.18
8	$LVHS_2$	13.39	13.62	3.07	1.81	5.44	0.17	55.51	6.99	0.00	0.23	19.07	−20.02	−0.95	0.23
9	$LVHS_2$	7.05	21.47	6.14	3.40	0.00	0.00	60.33	1.22	0.00	0.39	16.32	−17.78	−1.46	0.29
10	$LVHS_2$	9.39	18.63	7.36	3.39	0.84	0.00	56.09	3.44	0.75	0.11	17.47	−17.97	−0.49	0.40
11	$LVHS_2$	0.00	25.78	8.58	3.11	0.00	0.00	61.63	0.47	0.12	0.31	15.17	−17.68	−2.51	0.33
12	$LVHS_2$	0.00	24.80	8.58	0.57	1.48	0.98	62.85	0.47	0.27	0.00	15.69	−18.02	−2.33	0.35
13	$LVHS_3$	18.44	12.67	0.92	3.73	2.61	1.10	55.29	5.24	0.00	0.00	20.32	−18.86	1.46	0.07
14	$LVHS_3$	20.06	15.89	2.56	4.81	0.91	0.14	47.89	7.74	0.00	0.00	21.07	−18.34	2.73	0.16
15	$LVHS_3$	9.13	9.52	2.31	6.14	3.87	2.93	60.02	4.01	0.00	0.00	19.56	−19.43	0.13	0.24
16	$LVHS_3$	20.14	10.92	1.16	4.39	0.54	0.36	57.79	4.70	0.00	0.00	18.30	−19.23	−0.93	0.11
17	$LVHS_3$	21.95	10.69	2.11	2.96	0.21	1.14	54.52	5.28	1.03	0.00	19.57	−18.67	0.90	0.20
							Mole percent								
1	$LVHS_1$	0.14	5.61	0.10	3.73	0.00	0.12	17.54	0.44	0.26	0.00				
2	$LVHS_1$	2.06	8.24	0.24	0.18	0.75	0.66	18.53	0.43	0.04	0.00				
3	$LVHS_1$	2.06	9.11	0.80	0.18	0.75	0.59	17.40	0.43	0.04	0.00				
4	$LVHS_2$	0.71	9.25	2.39	0.56	0.74	0.00	17.03	0.39	0.00	0.00				
5	$LVHS_2$	0.31	7.16	3.07	0.66	0.91	0.59	17.10	0.35	0.20	0.00				
6	$LVHS_2$	0.21	11.03	1.69	0.51	0.74	0.59	16.67	0.62	0.00	0.00				
7	$LVHS_2$	0.00	10.49	1.13	0.91	1.49	0.00	17.07	0.66	0.00	0.02				
8	$LVHS_2$	3.34	5.93	0.79	0.32	2.24	0.06	15.66	2.18	0.00	0.04				
9	$LVHS_2$	1.76	9.34	1.57	0.61	0.00	0.00	17.02	0.38	0.00	0.06				
10	$LVHS_2$	2.34	8.10	1.88	0.61	0.35	0.00	15.82	1.07	0.14	0.02				
11	$LVHS_2$	0.00	11.21	2.19	0.56	0.00	0.00	17.38	0.15	0.02	0.05				
12	$LVHS_2$	0.00	10.79	2.19	0.10	0.61	0.36	17.73	0.15	0.05	0.00				
13	$LVHS_3$	4.60	5.51	0.24	0.67	1.07	0.41	15.60	1.63	0.00	0.00				
14	$LVHS_3$	5.01	6.91	0.66	0.86	0.37	0.05	13.51	2.41	0.00	0.00				
15	$LVHS_3$	2.28	4.14	0.59	1.10	1.59	1.09	16.93	1.25	0.00	0.00				
16	$LVHS_3$	5.03	4.75	0.30	0.79	0.22	0.13	16.30	1.47	0.00	0.00				
17	$LVHS_3$	5.48	4.65	0.54	0.53	0.09	0.42	15.38	1.65	0.19	0.00				

ΣZ^+ = sum of cation charges, ΣZ^- = sum of cation charges

TABLE 4. Oxygen Isotope Results of the Mineralized Group Quartz Veins

Sample no.	Mineral	Vein type	Alteration type	Yield values	$\delta^{18}O$ (‰)
25-437	Quartz	I	Potassic	16.5	9.5
25-466	Quartz	I	Potassic	16.9	9.5
25-487	Quartz	I	Potassic	15.9	9.5
34-498	Quartz	II	Transition	16.2	10.1
36-213	Quartz	III	Phyllic	16.0	10.3

tain up to 0.6 *m* S. The molality of Cu varied from 0.02 to 0.06 and compares favorably with estimates of 0.02 to 0.04 *m* obtained by relating the volume of the daughter mineral to the volume of fluid in eight $LVHS_2$ inclusions.

Stable Isotope Geochemistry

Oxygen isotopes

Oxygen isotope analyses were conducted on five samples of quartz from group I, II, and III veins in the potassic, transition, and phyllic alteration zones (Table 4). Quartz grains were separated using both heavy liquid and handpicking methods. The $^{18}O/^{16}O$ ratios were determined by D. Pezderic at the Department of Geological Sciences, University of Saskatchewan, employing methods similar to those described by Sheppard and Taylor (1974). The values are precise to a level of 0.1 per mil. The $\delta^{18}O$ values of quartz are the same (9.5‰) in all samples (3) from the potassic alteration zone (group I veins) and are slightly higher for the transition (group II veins) and phyllic (group III veins) zone samples at 10.1 and 10.3 per mil, respectively. The corresponding $\delta^{18}O$ values for the fluids in group I and II quartz veins are 6.5 to 7.1 per mil, assuming an average temperature of vein formation of 450°C, and 5.2 per mil in group III quartz veins assuming an average temperature of 360°C (discussed later). These values are consistent with a dominantly magmatic source for the vein-forming fluids. It should be noted, however, that the group III veins are interpreted to represent reopened group II veins, and it is thus possible that the $\delta^{18}O$ values for the group III vein samples are related to their earlier history.

Sulfur isotopes

Sulfur isotope analyses were performed on 15 pyrite, anhydrite, chalcopyrite, and molybdenite samples separated from group I, II, and III veins. Mineral separation was performed by heavy liquids and by handpicking. The purity of the separated minerals was confirmed by examination with a binocular microscope. The analyses were performed at the Stable Isotope Laboratory at the University of Ottawa and have a precision of 0.1 per mil.

Sulfur isotope data are reported in Table 5. Although the data are limited, there is no evidence that any of the minerals vary systematically in isotopic composition with respect to mineral paragenesis or alteration. The four molybdenite samples analyzed have $\delta^{34}S$ values between −0.3 and −2.0 per mil, the three chalcopyrite samples have $\delta^{34}S$ values of −1.4 to −1.6 per mil, the five pyrite samples have $\delta^{34}S$ values ranging from −0.5 to −3 per mil, and the two anhydrite

TABLE 5. Sulfur Isotope Data from Sulfate and Sulfide Minerals in Veins from the Sungun Deposit

Sample no.	Vein stage	$\delta^{34}S$ (‰) Ccp	Py	Mo	Anh	$\Delta^{34}S_{py\text{-}ccp}$ (‰)	T (°C)	$\Delta^{34}S_{ccp\text{-}mo}$ (‰)	T (°C)	$\Delta^{34}S_{anh\text{-}py}$ (‰)	T (°C)	$\Delta^{34}S_{anh\text{-}mo}$ (‰)	T (°C)	$\Delta^{34}S_{anh\text{-}ccp}$ (‰)	T (°C)
25-437	I		−1.5	−0.8	11.8					13.3	465 ± 20	12.6	470 ± 20		
25-461	I			−1.1	11.8							12.9	460 ± 20		
25-466	I		−1.7	−0.3	11.8					13.5	480 ± 20	12.1	485 ± 20		
106-529	I	−1.4		−2	11.8			0.6	475 ± 20			13.8	455 ± 20	13.2	470 ± 20
33-125	II	−1.6													
25-397	II		−1.5												
36-213	III	−1.6	−0.5		11.6	1.1	360 ± 20			12.1	470 ± 20			13.2	470 ± 20
21-127	III		−3		11.6					14.6	450 ± 20				

Abbreviations: anh = anhydrite, ccp = chalcopyrite, mo = molybdenite, py = pyrite

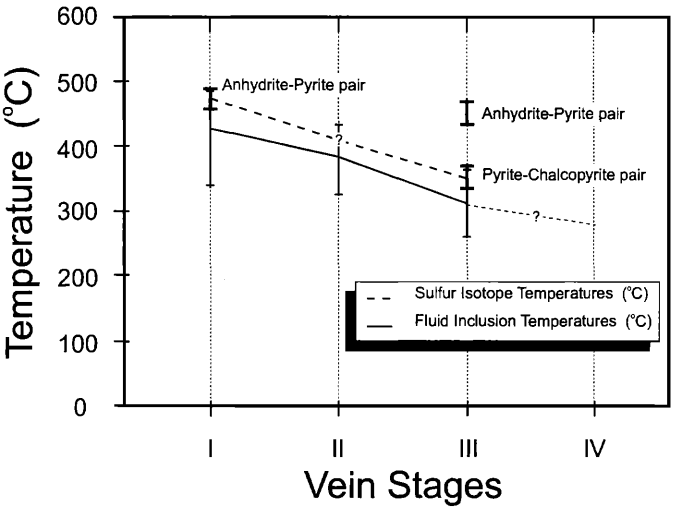

FIG. 15. Comparison of vein formation temperatures calculated from fluid inclusion microthermometry, with sulfur isotope fractionation. The temperatures estimated by the two different methods are similar except for group III veins where temperatures based on S isotope fractionation between anhydrite and pyrite are anomalously high.

samples have nearly identical $\delta^{34}S$ values of 11.6 and 11.8 per mil. In the group I and II veins, the textural relationships between the sulfide (i.e., pyrite, chalcopyrite, and molybdenite) and anhydrite show that they have been coprecipitated. For group I veins, the only mineral pairs for which data are available from which to calculate temperature are pyrite-molybdenite, anhydrite-pyrite, and anhydrite-molybdenite. The temperatures calculated from $\delta^{34}S$ for anhydrite-pyrite, anhydrite-molybdenite, and anhydrite-chalcopyrite pairs from the group I veins using the fractionation equations given in Barnes (1979) range from 450 ± 10° to 485 ± 10°C. The $\delta^{34}S$ value for molybdenite-pyrite is too small to permit reliable calculation of temperature. Trapping temperatures of primary fluid inclusions in group I quartz veins vary between 330° ± 10° and 500° ± 10°C. The isotopic temperatures from S isotope geothermometry are therefore in good agreement with the fluid inclusion data and suggest attainment of sulfur isotope equilibrium (Fig. 15). Unfortunately $\delta^{34}S$ data for group II veins were restricted to values for chalcopyrite and pyrite from separate samples, and a temperature for these veins could not be calculated. However, the $\delta^{34}S$ values are very similar to those for the corresponding minerals in group I veins, suggesting that temperatures were also similar. Anhydrite-pyrite, anhydrite-chalcopyrite, and pyrite-chalcopyrite pairs for group III veins yielded temperatures of 450° ± 10°C, 470° ± 10°C, and 360° ± 10°C, respectively. We interpret this disagreement to reflect earlier deposition of anhydrite as a higher temperature group II vein mineral in a vein that was subsequently reopened to allow entry of group III vein-forming fluids. This interpretation is supported by textural relationships which suggest that the sulfide minerals were precipitated later than the anhydrite.

Discussion

Pressure-temperature conditions

The maximum pressure of fluid entrapment can be calculated from the estimated thickness of the overlying rock column at the time of intrusion, which at Sungun is estimated to have been between 1.5 and 2.0 km. The latter represents ~500 m of Cretaceous limestone, plus 1,000 to 1,500 m of lower Tertiary volcanic, volcanoclastic, and related sedimentary rocks. This corresponds to a lithostatic pressure of 400 to 500 bars (assuming an average rock density of 2.7 g/cm^3) and a hydrostatic pressure of 150 to 200 bars (assuming a fluid density near 1 g/cm^3).

Estimates of the temperatures of fluid entrapment can be made from the microthermometric and sulfur isotopec data. In the case of LVHS inclusions the microthermometric data also permit independent estimates of pressure. As discussed earlier, the various fluid inclusion types are interpreted to represent three populations which, in principle, could have been trapped under different pressure-temperature conditions. $LVHS_1$ fluid inclusions occur with VL inclusions in group I quartz veins associated with potassic alteration, and together with $LVHS_2$ fluid inclusions, define fluid population I. The homogenization temperatures for type $LVHS_1$ inclusions (generally $T_{h_{L\text{-}V}} > T_{m_{halite}}$) vary between 330° and ~500°C, and for coexisting VL inclusions, between 400° and 500°C (Fig. 16); $LVHS_2$ inclusions homogenize at temperatures from 280° to 500°C (generally $T_{h_{L\text{-}V}} < T_{m_{halite}}$). Similar temperatures are predicted by the sulfur isotopec data (Fig. 15). At these temperatures the maximum pressure for the coexistence of these two fluid inclusion types (bubble point curve) is approximately 300 to 400 bars. On the other hand, the existence of LVHS fluid inclusions with $T_{m_{halite}} >> T_{h_{L\text{-}V}}$ (mainly $LVHS_2$) implies that pressure was locally or temporarily much higher, assuming that the high values of $T_{m_{halite}}$ do not reflect accidental trapping or metastable dissolution of halite (cf. Chivas and Wilkins, 1977). If a single outlier is excluded, the pressures estimated for inclusions with $T_{m_{halite}} >> T_{h_{L\text{-}V}}$ range as high as 800 bars, which exceeds the lithostatic pressure of 400 to 500 bars. We therefore propose that fluid pressure exceeded lithostatic pressure and that pressure generally oscillated between 150 to 200 bars (hydrostatic) and >500 bars in response to repeated cracking and sealing of the rock at a temperature of ~450°C.

$LVHS_3$ and VL inclusions are spatially associated in the higher levels of the deposit (phyllic alteration zone) where they are interpreted to constitute fluid inclusion population II. In group I and II veins, $LVHS_3$ inclusions homogenize by vapor disappearance after halite dissolution at a modal temperature of 350°C. Based on data from Sourirajan and Kennedy (1962) and Chou (1987) for the NaCl-H_2O system, the corresponding fluid pressure was ~200 bars. VL inclusions (vapor rich) homogenize to a vapor at between 380° and 520°C, i.e., at significantly higher temperatures than $LVHS_3$ inclusions. We attribute this to heterogeneous entrapment of liquid and vapor during boiling. In group III veins, the $LVHS_3$ inclusions homogenize at temperatures <300°C by both vapor disappearance and halite dissolution. Fluid II was thus trapped at considerably lower temperatures than fluid I (~350° vs. 350°–500°C) and underwent cooling with the development of a progressively more open fracture system represented by group III veins. The pressure was dominantly hydrostatic (150–200 bars).

Fluid inclusion population III is represented by secondary

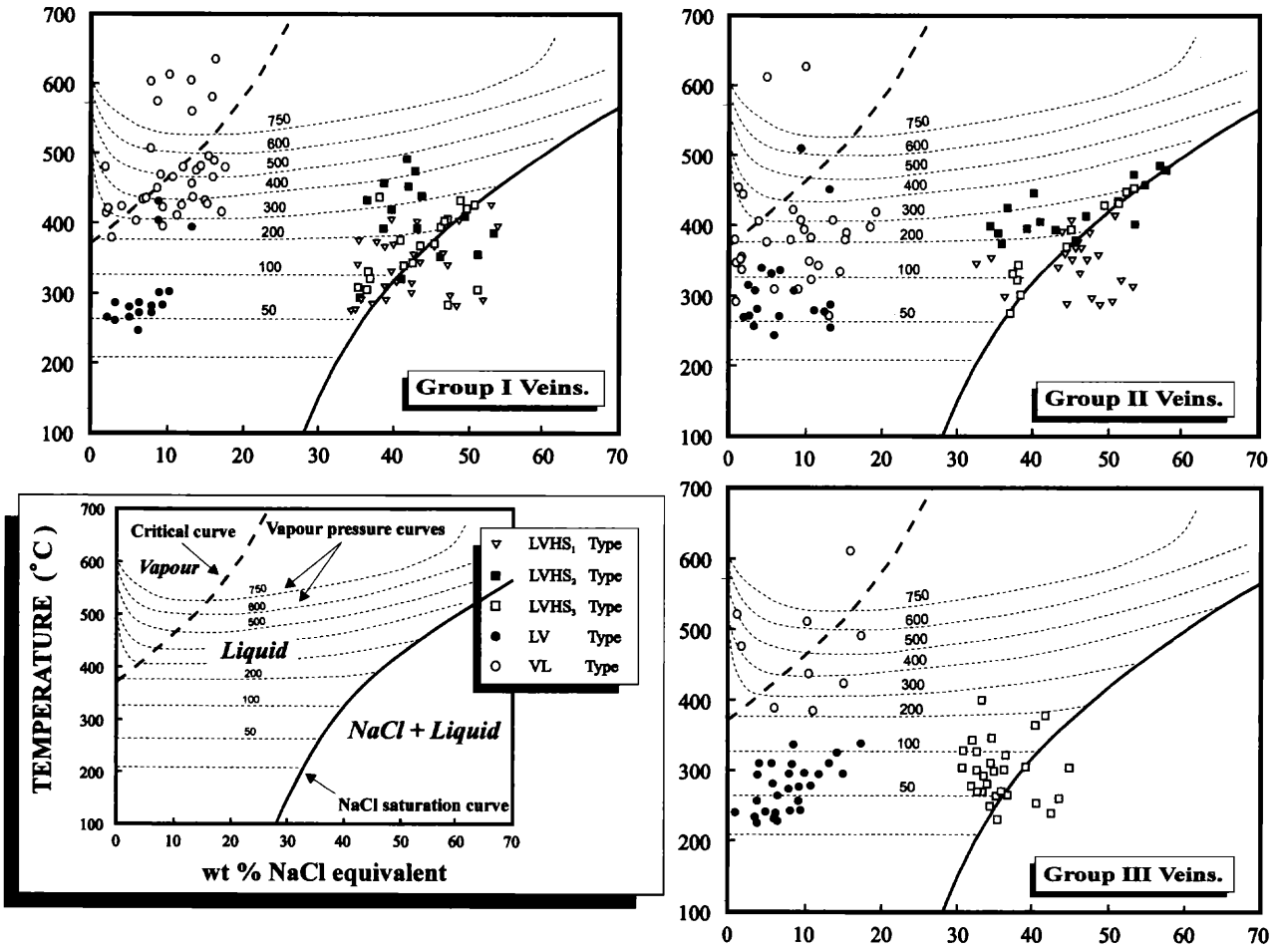

FIG. 16. Liquid-vapor homogenization temperature vs. salinity plotted on a section from the NaCl-H_2O system (halite saturation and critical curves from Chou, 1987).

LV fluid inclusions, which occur largely in group II and group III veins and homogenize to liquid at temperatures between 240° and 330°C. Using the data of Chou (1987), the minimum corresponding pressure is between ~30 and ~120 bars.

Fluid evolution

The high trapping temperatures (350° to >500°C) and high salinity of $LVHS_1$ and $LVHS_2$ fluid inclusions suggest that fluid population I probably represents an orthomagmatic fluid. We propose that this fluid exsolved as a high-density phase from a diorite-granodiorite magma (the solidus temperature of this magma and emplacement pressure are above the critical point curve for high-salinity fluids in the system NaCl-KCl-H_2O), and subsequently saturated with halite and boiled. Furthermore, we propose that the $LVHS_2$ fluid inclusions generally represent the preboiled fluid, and the $LVHS_1$ and VL inclusions, the high- and low-density products of boiling, respectively.

The conclusion that $LVHS_2$ fluid inclusions represent the preboiled fluid is based on the fact that their compositions, as discussed previously, delineate a so-called halite trend on an NaCl-KCl-H_2O diagram (Fig. 14), similar to those reported for other porphyry copper deposits (e.g., Eastoe, 1978; Ahmad and Rose, 1980; Wilson et al., 1980; Quan et al., 1987). These trends have been interpreted by Cloke and Kesler (1979) as being due to early saturation of the fluid with halite and subsequent trapping of the fluid over an interval of cooling. We propose that this was also the case for the $LVHS_2$ fluid inclusions, i.e., that they were largely trapped before the onset of widespread boiling. However, the displacement of the trend toward the H_2O apex and the existence of $LVHS_2$ fluid inclusions which homogenize by vapor disappearance suggest that there was some boiling even at this early stage of fluid evolution. The halite trend, represented by fluid inclusions that homogenize by halite dissolution, is described by the path M-N-O in Figure 17. Liquids trapped between points N and O would be on the halite trend because they are in equilibrium with halite. By contrast, $LVHS_2$ fluid inclusions, which homogenize by vapor disappearance ($T_{h_{L\text{-}V\rightarrow L}} > T_{m_{halite}}$), probably record sudden lowering of pressure from M-N-O along N-P or N-Q (isothermal) and boiling. This decompression most likely occurred episodically due to fluid overpressuring (recorded by $LVHS_2$ fluid inclusions which appear to have been trapped at pressures greater than lithostatic; see previous section), hydrofracturing, and resultant sharp changes from supralithostatic to hydrostatic conditions.

Our interpretation that $LVHS_1$ fluid inclusions are the products of boiling is supported by the facts that they almost invariably homogenized by vapor disappearance and that they are commonly associated spatially with VL inclusions. We conclude that $LVHS_1$ and VL fluid inclusions record a later stage in the evolution of the Sungun hydrothermal system than that of the $LVHS_2$ fluid inclusions, i.e., a stage when conditions were closer to hydrostatic and fluid I boiled extensively.

We propose that the source of fluid population II ($LVHS_3$ and VL fluid inclusions) was also mainly orthomagmatic (high salinity), but that this fluid circulated at lower temperature than fluid I (~350°C vs. 350°–500°C) and mixed with an external fluid. Mixing is suggested by the high concentrations of Ca measured in residues of decrepitated inclusions; these could have been introduced from the surrounding limestones. This is also suggested by a weak trend from higher temperature and higher salinity to lower temperature and lower salinity in going from $LVHS_3$ to LV fluid inclusions (Fig. 16). Coexistence of $LVHS_3$ fluid inclusions (which homogenize largely by vapor disappearance) with VL fluid inclusions indicates that fluid II boiled extensively.

Fluid III (LV inclusions) circulated mainly in group II and III veins at temperatures from 330° to 240°C. We propose that the source of fluid III was mainly meteoric water and that it mixed to variable degrees with magmatic fluids. This conclusion is based on the decrease in salinity from 18 wt percent down to 1 wt percent NaCl equiv (Fig. 16) in LV fluid inclusions and the corresponding decrease in homogenization temperature.

Fluids II and III commonly occur together in group II and III veins. We interpret this to record the downward movement of fluid III (dominantly meteoric), which initially was at conditions indicated by point X in Figure 17, and its subsequent evolution along a path of increasing temperature due to mixing with orthomagmatic fluids, which originated at point M. At point Y the fluid reached its maximum depth and subsequently ascended along an adiabatic cooling curve (Y-Z).

The fluid inclusion data discussed above indicate that there was a general decrease in temperature and salinity with time in the fluid responsible for ore deposition. Homogenization temperatures of fluid inclusions decrease from around 500°C in group I veins to about 240°C in group III veins, and the

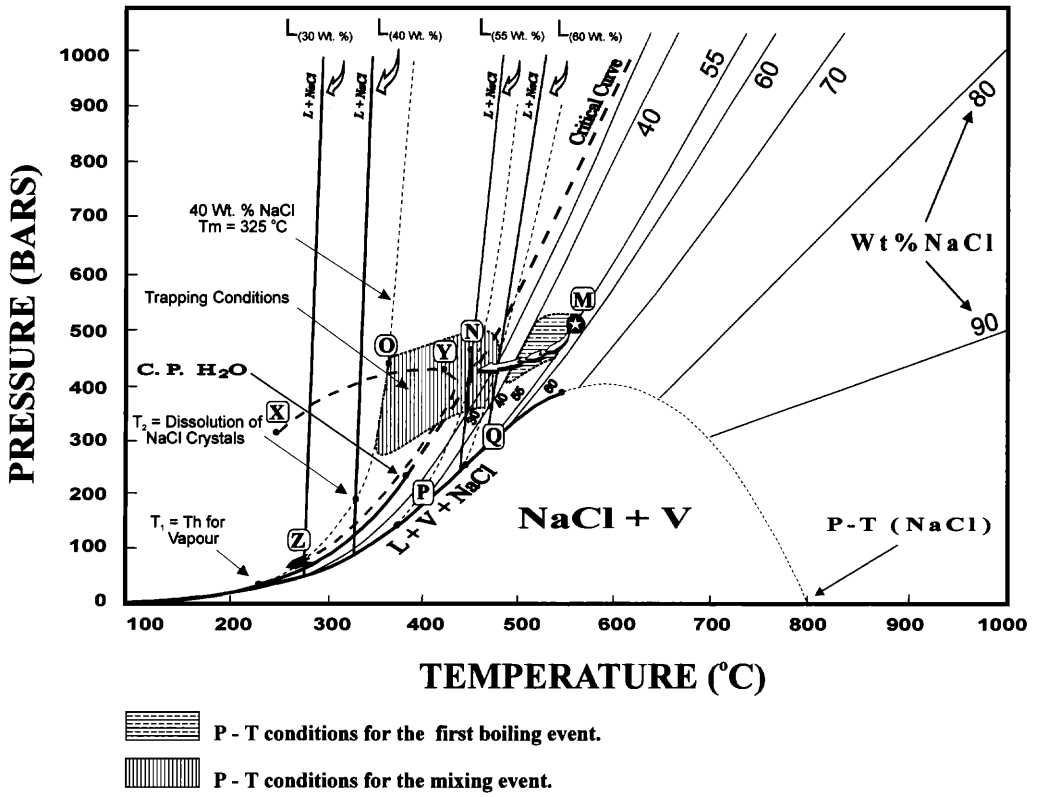

FIG. 17. Pressure-temperature diagram for the system NaCl-H_2O showing the proposed mechanisms for the formation of the LVHS fluid inclusions VL and lower salinity LV inclusions. The LVHS inclusions are envisaged to represent part of a boiling fluid of orthomagmatic origin first trapped at a temperature of approximately 540°C and pressure of 500 bars (M). M-N-O is the path that explains the $LVHS_1$ and $LVHS_2$ inclusions which homogenize by halite disappearance. Liquids trapped between points N and O are in equilibrium with halite. To form the $LVHS_3$ fluid inclusions which homogenize by vapor disappearance, it is necessary to invoke sudden lowering of pressure along N-P or N-Q (isothermal) until the fluid is in equilibrium with vapor (see text for more information). Point X represents the assumed initial P-T conditions for the evolved meteoric fluid. This fluid moved downward into the system and mixed with orthomagmatic fluids, thereby evolving along a path of increasing temperature and pressure. At point Y the fluid reached its maximum depth and subsequently ascended along an adiabatic cooling curve (Y-Z). Trapping of this fluid led to the formation of LV inclusions. Abbreviations: C.P. H_2O = critical point of water, L = liquid, NaCl = halite, V = vapor. Diagram modified after Chou (1987), with liquidus curves from Bodnar (1992).

salinity of LVHS fluid inclusions decreases from 55 wt percent NaCl equiv in group I veins to 33 wt percent equiv in group III veins; the salinity of LV inclusions decreases from 18 to 1 wt percent NaCl equiv. These changes in fluid temperature and salinity reflect the cooling of a saline aqueous fluid exsolved from a diorite-granodiorite magma, and its subsequent boiling and mixing with meteoric waters as conditions evolved from being dominantly lithostatic to dominantly hydrostatic.

Alteration and mineralization

The presence of molybdenite and anhydrite in group I veins, chalcopyrite and anhydrite in group II veins, and chalcopyrite and anhydrite in $LVHS_1$ and $LVHS_2$ inclusions from group I and II veins suggests that fluid I was responsible for the transport and eventual deposition of Mo, Cu, Fe, and S. Molybdenite formed at the margins of the group I veins, where its deposition was probably controlled by the temperature decreasing from ~520° to ~450°C. If Mo was transported as the complex $KMoO_4^0$, it is also possible that deposition occurred due to destabilization of this complex as a result of the transfer of K^+ to the surrounding potassic alteration halos (Nast and Williams-Jones, 1991). The cooling (and K^+ transfer) stabilized K feldspar at the expense of plagioclase, and biotite at the expense of hornblende; the K/Na ratio was approximately 0.3. The rarity of chalcopyrite in group I veins and its abundance in group II veins indicates that physicochemical conditions only became appropriate for bulk Cu deposition during formation of group II veins, i.e., after some evolution of the hydrothermal system. The occurrence of anhydrite in the hypogene mineral assemblage can be explained by the hydrolysis of SO_2 upon cooling: $4SO_2 + 4H_2O = 3H_2SO_4 + H_2S$. Thus, the breakdown of SO_2, which is believed to occur around 400°C (Burnham, and Ohmoto, 1980; Burnham, 1981), is a possible source for both sulfate (to form anhydrite) and sulfide (to form molybdenite, pyrite, and chalcopyrite).

A fluid of mainly mixed meteoric and magmatic origin circulated later in the central part of the stock, at temperatures up to 420°C. Late fractures, or reopened veins, provided the pathways for this fluid to circulate in the system. It is proposed that the low K/Na ratio (<0.2) and relatively high temperature of this fluid caused destabilization of the previously formed K feldspar in the potassic alteration zone and its replacement by albite (transition zone). The fluid also dissolved earlier formed copper sulfide minerals (higher f_{O_2}) and remobilized Cu to the upper levels of the intrusion. There it boiled causing extensive sericitization and silicification, and reprecipitation of the Cu as chalcopyrite all in response to the resultant cooling. During potassic alteration and mainstage Cu-Mo mineralization, (380°–520°C), the peripheral part of the stock was altered propylitically at lower temperatures (240°–420°C). The circulation of fluid III, which did not penetrate into the hotter central part of the intrusion, caused this alteration zone. This fluid also may have caused some of the argillic alteration, in which almost all the feldspars were altered to kaolinite and other clay minerals.

Conclusions

The multiple intrusions of dioritic and granodioritic to quartz-monzonitic rocks at Sungun indicate a long-lived intrusive episode associated with repeated fracturing and hydrothermal activity. Mineralogical, fluid inclusion, and isotopic analyses from the deposit indicate three distinct hydrothermal fluids. The first hydrothermal fluid caused potassic alteration and Cu ± Mo mineralization. This fluid was characterized by high temperatures and moderate to high salinities, and was probably magmatically derived. It was responsible for the wide distribution of group I and II mineralized quartz veins, at temperatures ranging from 380° to 520°C, and boiled episodically. The data from oxygen isotope analyses suggest a magmatic source for the corresponding hydrothermal mineralization in those veins. The second hydrothermal fluid (fluid II) was formed mainly by the mixing of magmatic fluid, at moderate to low temperatures (up to 420°C), with a predominantly meteoric fluid (fluid III), and also boiled. This fluid was responsible for the transition and sericitic alteration zones in the lower and upper portion of the stock, respectively, and also remobilized Cu upward. The third hydrothermal fluid (fluid III) consisted of low-temperature, low- to moderate-salinity (1–18 wt % NaCl equiv) oxidized meteoric water, which was responsible for peripheral propylitic alteration in a zone outside the core of potassically altered rock, and possibly argillic alteration when it was allowed to penetrate into the system. Final supergene enrichment of copper minerals was very limited and consists of a thin blanket (up to 45 m) containing covellite, chalcocite, and digenite, located below an intensely altered cap.

Acknowledgments

The Ahar Copper Company provided access to the deposit and logistical support, including accommodation and transportation. Financial support for the research was provided by a scholarship from the Iranian Ministry of Culture and Higher Education to A.H. and a Natural Sciences and Engineering Research Council (Canada) grant to A.E.W.-J. We would like to thank C.H. Gammons, C. Eastoe, R. Herrington, and J. Clark for their helpful suggestions and constructive criticisms.

December 16, 1996; March 3, 1998

REFERENCES

Ahmad, S.N., and Rose, A.W., 1980, Fluid inclusions in porphyry and skarn ore at Santa Rita, New Mexico: Economic Geology, v. 75, p. 229–250.

Barnes, H.L., 1979, Geochemistry of hydrothermal ore deposits: New York, Wiley Interscience, 798 p.

Bazin, D., and Hübner, H., 1969, Copper deposits in Iran: Iran Geological Survey, Ministry of Economy Report 13.

Berberian, M., 1983, The southern Caspian: A compressional depression floored by a trapped, modified oceanic crust: Canadian Journal of Earth Sciences, v. 20, p. 163–183.

Berberian, M., and King, G.C., 1981, Towards a paleogeography and tectonic evolution of Iran: Canadian Journal of Earth Sciences, v. 18, p. 210–265.

Bodnar, R.J., 1992, Experimental determination of the liquidus and isochores of a 40 wt % $NaCl-H_2O$ solution using synthetic fluid inclusions [abs]: Pan-American Conference on Research in Fluid Inclusions (PACROFI IV), 4th, Lake Arrowhead, CA, May 22–25, 1992, Program and abstracts, v. 4, p. 14.

Burnham, C.W., 1981, Physiochemical constraints on porphyry mineralization: Arizona Geological Society Digest, no. 14, p. 71–77.

Burnham, C.W., and Ohmoto, H., 1980, Late-stage processes of felsic magmatism, *in* Ishihara, S., and Takenouchi, S., eds., Granitic magmatism and related mineralization: Tokyo, Society of Mining Geologists of Japan, p. 1–12.

Chivas, A.R., and Wilkins, W.T., 1977, Fluid inclusion studies in relation to

hydrothermal alteration and mineralization at the Koloula porphyry copper prospect, Guadalcanal: ECONOMIC GEOLOGY, v. 72, p. 153–169.

Chou, I.M., 1987, Phase relations in the system NaCl-KCl-H_2O. III: Solubilities of halite in vapor-saturated liquids above 445°C and redetermination of phase equilibrium properties in the system NaCl-H_2O to 1000°C and 1500 bars: Geochimica et Cosmochimica Acta, v. 51, p. 1965–1975.

Cloke, P.L., and Kesler, S.E., 1979, The halite trend in hydrothermal solutions: ECONOMIC GEOLOGY, v. 74, p. 1823–1831.

Eastoe, C.G., 1978, A fluid inclusion study of the Panguna porphyry copper deposit, Bougainville, Papua New Guinea: ECONOMIC GEOLOGY, v. 73, p. 721–748.

Emami, H., 1992, Geology of the Sungun copper deposit: Sungun Copper Company, Internal reports,

Etminan, H., 1977, A porphyry copper-molybdenum deposit near the Sungun village: Iran Geological Survey Internal Report, 24 p.

——1978, Fluid inclusion studies of the porphyry copper ore bodies at Sar-Cheshmeh, Darreh Zar and Mieduk (Kerman region, southeastern Iran) and porphyry copper discoveries at Sungun, Gozan, and Kighal, Azarbaijan region (northwestern Iran)[abs.]: International Association on the Genesis of Ore Deposits (IAGOD), 5th, Abstracts, p. 88.

Gustafson, L.B., and Hunt, J.P., 1975, The porphyry copper deposit at El Salvador, Chile: ECONOMIC GEOLOGY, v. 70, p. 857–912.

Haynes, F.M., 1984, Vein densities in drill core, Sierrita porphyry copper deposit, Pima County, Arizona: ECONOMIC GEOLOGY, v. 79, p. 755–758.

Haynes, F.M., Sterner, S.M., and Bodnar, R.J., 1988, Synthetic fluid inclusions in natural quartz. IV. Chemical analyses of fluid inclusions by SEM/EDA: Evaluation of method: Geochimica et Cosmochimica Acta, v. 52, p. 969–977.

Hezarkhani, A., 1997, Physicochemical controls on alteration and copper mineralization in the Sungun porphyry copper deposit, Iran: Unpublished Ph.D. thesis, McGill University, 281 p.

Linke, W.F., 1965, Solubilities of inorganic and metal organic compound,4th ed.: Washington, D.C., American Chemical Society, v. 2.

Lowell, J.D., and Guilbert, J.M., 1970, Lateral and vertical alteration-mineralization zoning in porphyry ore deposits: ECONOMIC GEOLOGY, v. 65, p. 373–408.

Mehrpartou, M., 1993, Contributions to the geology, geochemistry, ore genesis and fluid inclusion investigations on Sungun Cu-Mo porphyry deposit (north-west Iran): Unpublished Ph.D. thesis, Hamburg University, 245 p.

Nast, H.J., and Williams-Jones, A.E., 1991, The role of water-rock interaction and fluid evolution in forming the porphyry-related Sisson Brook W-Cu-Mo deposit, New Brunswick: ECONOMIC GEOLOGY, v. 86, p. 302–317.

Niazi, M., and Asoudeh, I., 1978, The depth of seismicity in the Kermanshah region of the Zagros Mountains (Iran): Earth and Planetary Science Letters, v. 40, p. 270–274.

Pourhosseini, F., 1981, Petrogenesis of Iranian plutons: A study of the Natanz and Bazman intrusive complexes: Unpublished Ph.D. thesis, University of Cambridge, 315 p.

Quan, R.A., Cloke, P.L., and Kesler, S.E., 1987, Chemical analyses of halite trend inclusions from the Granisle porphyry copper deposit, British Columbia: ECONOMIC GEOLOGY, v. 82, p. 1912–1930.

Roedder, E., 1984, Fluid inclusions: Reviews in Mineralogy, v. 12, 644 p.

Shahabpour, J., 1982, Aspects of alteration and mineralization at the Sar-Cheshmeh copper-molybdenum deposit, Kerman, Iran: Unpublished Ph.D. thesis, Leeds University, 342 p.

——1994, Post-mineralization breccia dike from the Sar Cheshmeh porphyry copper deposit, Kerman, Iran: Exploration and Mining Geology, v. 3, p. 39–43.

Sheppard, S.M.F., and Taylor, H.P., Jr., 1974, Hydrogen and oxygen isotope evidence for the origin of water in the Boulder batholith and the Butte ore deposit, Montana: ECONOMIC GEOLOGY, v. 69, p. 926–946.

Sillitoe, R.H., 1973, Geology of the Los Pelambres porphyry copper deposit, Chile: ECONOMIC GEOLOGY, v. 68, p. 1–10.

Sourirajan, S., and Kennedy, G.C., 1962, The system H_2O-NaCl at elevated temperatures and pressures: American Journal of Science, v. 260, p. 115–141.

Sterner, S.M., Hall, D.L., and Bodnar, R.J., 1988, Synthetic fluid inclusions. V. Solubility of the system NaCl-KCl-H_2O under vapor-saturated conditions: Geochimica et Cosmochimica Acta, v. 52, p. 989–1005.

Stöcklin, J., 1977, Structural correlation of the Alpine ranges between Iran and Central Asia: Mem. H. Aser. Soc. Geol. France, pp. 333–353.

Stöcklin, J., and Setudenia, A., 1972, Lexique stratigraphique international: Paris, Asie Centre National de la Recherche Scientifique, v. 3, p. 75.

Titley, S.R., and Beane, R.E., 1981, Porphyry copper deposits: Part I. Geologic settings, petrology, and tectnogenesis: ECONOMIC GEOLOGY 75TH ANNIVERSARY VOLUME, p. 214–234.

Waterman, G.C., and Hamilton, R.L., 1975, The Sar-Cheshmeh porphyry copper deposit: ECONOMIC GEOLOGY, v. 70, p. 568–576.

Werre, R.W., Jr., Bodnar, R.J., Bethke, P.M., and Barton, P.B., 1979, A novel gas-flow fluid inclusion heating-freezing stage [abs.]: Geological Society of America Abstracts with Programs, v. 11, p. 539.

Whitney, J.A., 1989, Origin and evolution of silicic magmas: Ore deposition associated with magmas: Reviews in Economic Geology, v. 4, p. 183–201.

Wilson, J.W.J., Kesler, S.E., Cloke, P.L., and Kelly, W.C., 1980, Fluid inclusion geochemistry of the Granisle and Bell porphyry copper deposits, British Columbia: ECONOMIC GEOLOGY, v. 75, p. 45–61.